AGU PUBLICATIONS

Tectonics

RESEARCH ARTICLE
10.1002/2016TC004305

Key Points:
- We measured the two Pleistocene slip rates along the Boconó fault using ^{10}Be dating and Pleiades images (5.0–11.2 mm yr^{-1} and <20 mm yr^{-1})
- Boconó fault in the Yaracuy Valley accommodates 40 to 100% of the relative displacement between the Maracaibo Block and the South American plate
- The slip deficit in the Yaracuy Valley ranges from 1 to 4 m along the Boconó fault since the M_{WI} 7.4 event in 1812

Supporting Information:
- Supporting Information S1

Correspondence to:
L. Pousse-Beltran,
pousselea@gmail.com

Citation:
Pousse-Beltran, L., R. Vassallo, F. Audemard, F. Jouanne, J. Carcaillet, E. Pathier, and M. Volat (2017), Pleistocene slip rates on the Boconó fault along the North Andean Block plate boundary, Venezuela, *Tectonics*, *36*, 1207–1231, doi:10.1002/2016TC004305.

Received 13 JUL 2016
Accepted 25 MAY 2017
Accepted article online 30 MAY 2017
Published online 1 JUL 2017

Pleistocene slip rates on the Boconó fault along the North Andean Block plate boundary, Venezuela

Lea Pousse-Beltran[1], Riccardo Vassallo[1], Franck Audemard[2], François Jouanne[1], Julien Carcaillet[3], Erwan Pathier[3], and Matthieu Volat[3]

[1]Université Savoie Mont Blanc, ISTerre, CNRS, IRD, Le Bourget du Lac, France, [2]Venezuelan Foundation for Seismological Research, FUNVISIS, Caracas, Venezuela, [3]Université Grenoble Alpes, ISTerre, CNRS, Grenoble, France

Abstract The Boconó fault is a strike-slip fault lying between the North Andean Block and the South American plate which has triggered at least five $M_w > 7$ historical earthquakes in Venezuela. The North Andean Block is currently moving toward NNE with respect to a stable South American plate. This relative displacement at ~12 mm yr^{-1} in Venezuela (within the Maracaibo Block) was measured by geodesy, but until now the distribution and rates of Quaternary deformation have remained partially unclear. We used two alluvial fans offset by the Boconó fault (Yaracuy Valley) to quantify slip rates, by combining ^{10}Be cosmogenic dating with measurements of tectonic displacements on high-resolution satellite images (Pleiades). Based upon a fan dated at >79 ka and offset by 1350–1580 m and a second fan dated at 120–273 ka and offset by 1236–1500 m, we obtained two Pleistocene rates of 5.0–11.2 and <20.0 mm yr^{-1}, consistent with the regional geodesy. This indicates that the Boconó fault in the Yaracuy Valley accommodates 40 to 100% of the deformation between the South American plate and the Maracaibo Block. As no aseismic deformation was shown by interferometric synthetic aperture radar analysis, we assume that the fault is locked since the 1812 event. This implies that there is a slip deficit in the Yaracuy Valley since the last earthquake ranging from ~1 to 4 m, corresponding to a M_w 7–7.6 earthquake. This magnitude is comparable to the 1812 earthquake and to other historical events along the Boconó fault.

1. Introduction

Quantifying the loading strain rate along a fault within faulted system is the most essential aspect of active tectonism. This is of primary importance in the estimation of the accommodation of the deformation. Estimation of the loading strain rate can be achieved through two main methods: (i) geodetic investigations and (ii) geological studies. Geodetic studies are often used to constrain the large field velocity, allowing the estimation of the fault slip below locking depth [e.g., *Fialko*, 2006; *Reinoza et al*., 2015]. However, in regions with a sparse GPS network spanning several active faults, estimating the loading strain rate of an individual fault becomes impossible. In such regions, geological studies are mandatory to estimate slip rates smoothed over several seismic cycles on individual faults [e.g., *Ritz et al*., 1995, 2003; *Van der Woerd et al*., 2002; *Ferry et al*., 2007; *Frankel et al*., 2015]. Although it is quite challenging to find markers covering the whole fault zone, the obtained geological slip rate can be used to estimate slip deficit improving seismic hazard assessment [*Fattahi et al*., 2007; *Chevalier et al*., 2016].

This study focuses on an active fault in Venezuela, the Boconó fault, which is a ~ 500 km long NE-SW right-lateral strike-slip fault (Figure 1). This fault has triggered some of the $M_w > 7$ earthquakes of the regional historical seismicity [*Audemard*, 2016, and references therein], including the most destructive historical event in Venezuelan history in 1812 [*Audemard*, 2002, 2016; *Altez*, 2006; *Choy et al*., 2010]. The Yaracuy Valley is the least understood of the areas crosscut by the Boconó fault, due to (1) the existence of numerous faults, (2) the lack of GPS stations, and (3) the lack of instrumental seismicity (Figures 2 and 3). Nevertheless, there are numerous morphological markers offset by the Boconó fault, which allow to record the fault displacements, to determine the spatial pattern of the deformation and to estimate a Quaternary fault slip rate. To exploit these records, we (1) carried out detailed mapping of Quaternary deposits and morphotectonic markers offset by the fault on high-resolution images (Pleiades), (2) performed ^{10}Be terrestrial cosmogenic nuclide (TCN) dating on reliable offset markers, and (3) compared these results with new interferometric synthetic aperture radar (InSAR) measurements and published GPS velocities. Slip rates and surface ground motion obtained will then be used to quantify the slip deficit value. Finally, slip rates will be compared to other slip rates estimated on the North Andean Block in order to discuss the tectonic framework.

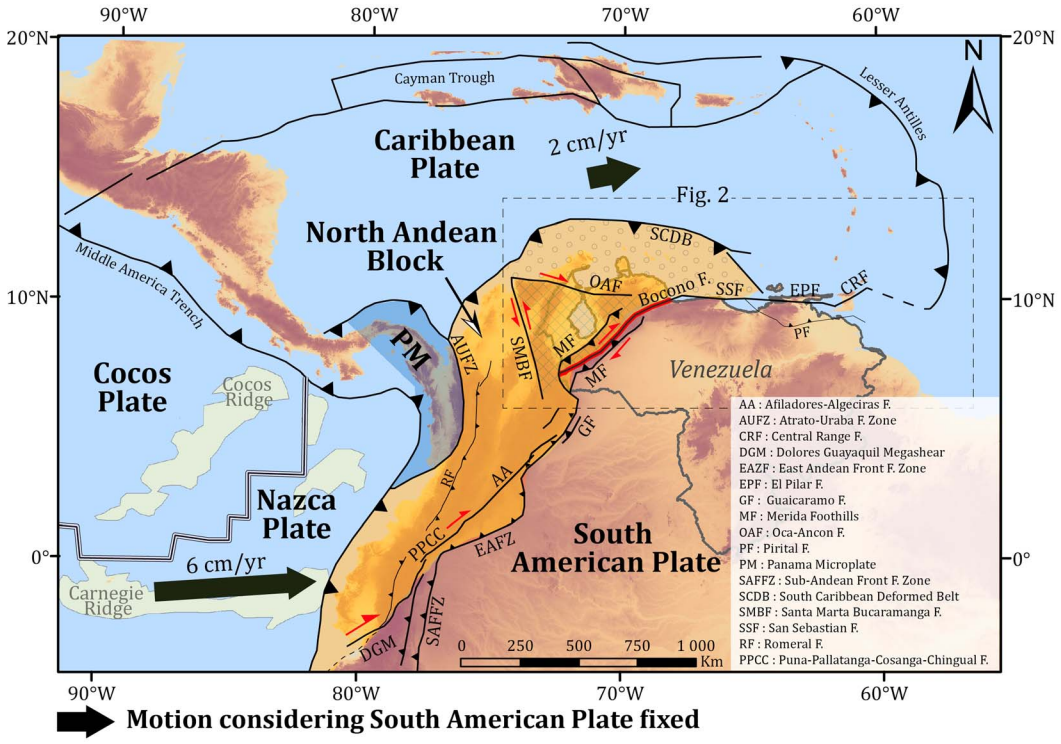

Figure 1. Geodynamic context of Venezuela. The North Andean Block (in yellow) composed of minor blocks accommodates part of the relative displacement between the South American, Nazca, and Caribbean plates. The Boconó fault is represented in red. This figure is based on *Trenkamp et al*. [2002], *DeMets et al*. [2010], *Egbue and Kellogg* [2010], and *Monod et al*. [2010].

2. Geodynamic Context

Geodynamics in the northern region of South America results from the interaction of three tectonic plates. If the South American plate is considered as being fixed, the Nazca and Caribbean plates move to the east at 6 cm yr^{-1} and at 2 cm yr^{-1}, respectively [*DeMets et al*., 2010]. Plate boundaries from Ecuador to Venezuela are difficult to identify, thus *Pennington* [1981] defined the North Andean Block as a wide zone composed of minor blocks (Figure 1). The North Andean Block bounded by several active faults is escaping to the NE relative to the stable South American plate [*Kellogg et al*., 1995; *Trenkamp et al*., 2002; *Egbue and Kellogg*, 2010; *Pérez et al*., 2011; *Alvarado*, 2012].

In Venezuela, the Northern Andean Block is composed of the Maracaibo Block and the Bonaire Block. These blocks are bounded by active faults (Figure 2a). Between the Maracaibo block and the South American plate lies the NE-SW Boconó fault system, whose strike-slip and thrust faults accommodate part of the regional transpressive tectonics [*Colletta et al*., 1997; *Audemard and Audemard*, 2002; *Pérez et al*., 2011; *Dhont et al*., 2012]. The right lateral strike-slip Boconó fault described by numerous geologists [*Rod*, 1956; *Bellizzia et al*., 1976; *Giraldo*, 1985; *Soulas*, 1986; *Ferrer*, 1991; *Beltran*, 1994; *Audemard*, 2005, 2009] has been divided into five segments (Boc-a, Boc-b, Boc-c, Boc-d and Boc-e) (Figure 2b) [*Audemard et al*., 2000]. These segments have been defined geometrically; a segment is a portion of the fault (or collection of faults) that has different characteristics (e.g., strike and segmentation) than adjacent portions [*Audemard et al*., 2000]. The segments are separated by the large ($>$ 4 km long) releasing bends and step overs (La Gonzalez, Mucuchies, Las Mesitas, and Cabudare in Figure 2b).

The fault is located between Colombia and Venezuela in the prolongation of the Colombian Llanos foothills (segment Boc-a). Starting from the SW and traveling NE, the fault crosscuts the Venezuelan Andes (Boc-b, Boc-c, and Boc-d segments) and then delimits the Yaracuy Valley (Boc-e) before curving E-W to connect with the San Sebastian-El Pilar fault system. Each of these segments has triggered at least one $M_w \geq 7$ historical

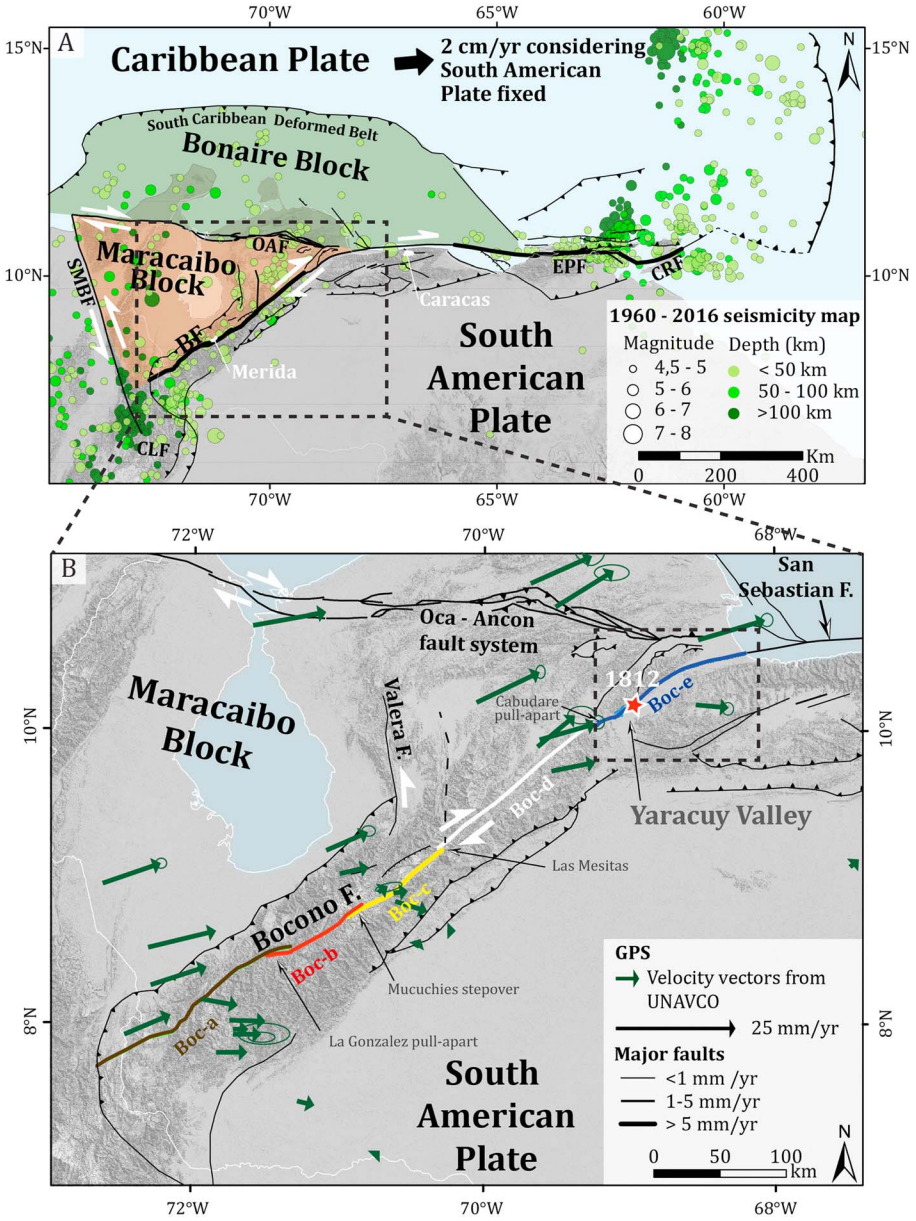

Figure 2. (a) Seismotectonic map of Venezuela: mapping of faults is based on *Audemard et al.* [2000], geodetic velocity is based on *DeMets et al.* [2010], and seismicity data are provided by the Advanced National Seismic System's comprehensive earthquake catalog (ANSS ComCat) [*U.S.Geological Survey*, 2017]. CLF: Colombian Llanos Foothills, CRF: Central Range Fault, EPF: El Pilar Fault, OAF: Ocá-Ancon Fault, SMBF: Santa Marta-Bucaramanga Fault, and SSF: San Sebastian Fault. (b) Seismotectonic map of western Venezuela, the fault slip rates come from Late Quaternary studies recompiled in *Audemard et al.* [2000]. The Boconó fault crosscuts the Venezuelan Andes and is divided into five segments [*Audemard et al.*, 2000]. The red star represents the supposed epicenter of the 1812 historical earthquake [*Choy et al.*, 2010]. Arrows display GPS velocities reported by *University NAVSTAR Consortium* (*UNAVCO*) [2017] relative to a stable South American plate. The dashed square is the location of Figure 3.

earthquake since 1600 [*Audemard*, 2014, 2016] and has also been well identified in the instrumental seismicity (Figures 2a and 3). Among the most destructive events, the 1812 earthquake affected the Boconó and San Sebastian faults and caused severe damage from Merida to Caracas, especially in the Yaracuy Valley [*Altez*, 2006; *Choy et al.*, 2010].

There is general agreement in geodetic studies that the Maracaibo Block is moving to the NNE at an average velocity of 12 mm yr^{-1} [*Pérez et al.*, 2001; *Weber et al.*, 2001; *Trenkamp et al.*, 2002; *Pérez et al.*, 2011; *Reinoza*,

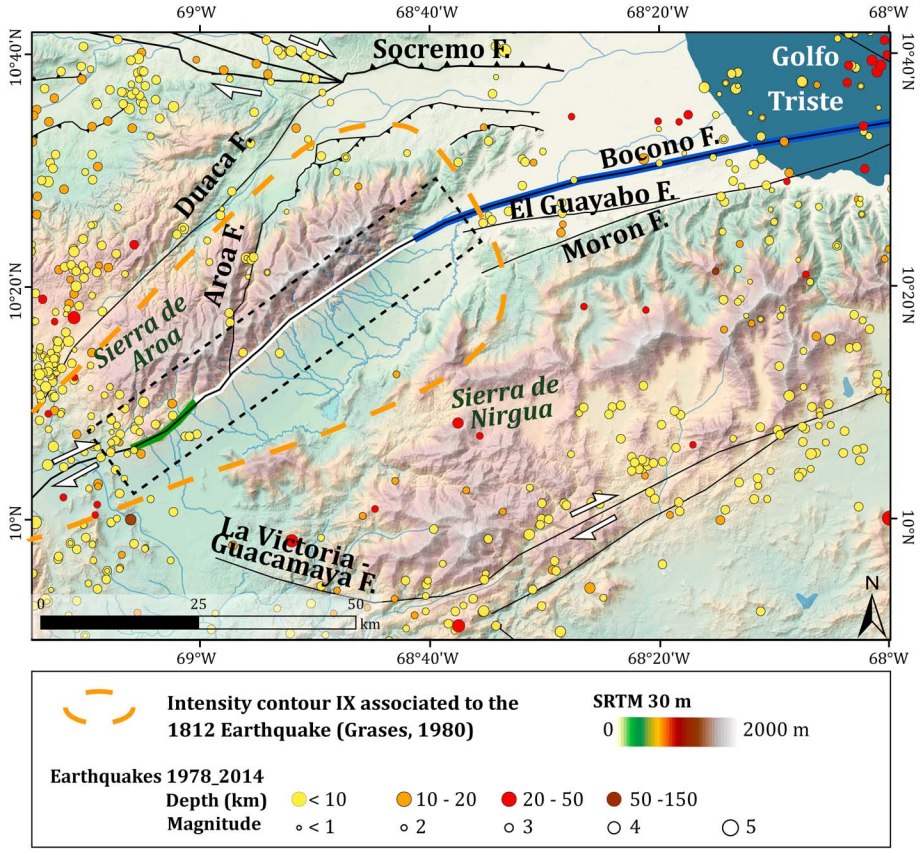

Figure 3. Seismotectonic context of the Yaracuy Valley. Fault mapping is based on *Audemard et al.* [2000]. The thick line represents the Boconó fault defined in *Audemard* [2016]: the blue portion is the Triste-Albarico segment, the white portion is the Albarico-La Virgen segment, and the green portion is the La Virgen-Yaritagua segment. The orange dashed line is IX intensity contour for the 1812 event drawn by *Grases* [1980]. Dots represent instrumental seismicity provided by FUNVISIS and by *International Seismological Centre* [2013]. The dashed rectangle represents Figure S2.

2014; *Symithe et al.*, 2015]. Therefore, assuming that the Santa Marta-Bucaramanga left-lateral fault (SMBF in Figure 2), the Ocá-Ancon right-lateral fault (OAF in Figure 2), and the Boconó fault are the main faults implies that the SMBF and the OAF have a slower geodetic slip rate than the Boconó fault (as shown by the block model of *Symithe et al.* [2015]). However, there are other active faults in this region, and the scarcity of geodetic velocities (Figure 2b) does not allow either fault geodetic slip rates or the locking depths of individual active faults (e.g., the Boconó fault section in the Yaracuy Valley) to be determined. In terms of Quaternary deformation, slip rates at four different locations along the central part of the Boconó fault have been estimated using absolute dating methods on offset markers [*Audemard et al.*, 1999; *Wesnousky et al.*, 2012; *Carcaillet et al.*, 2013]. These rates will be presented and discussed in section 6.3. However, there is no comparable data for the other Boconó fault segments, especially in Yaracuy Valley in the area of the epicenter of the 1812 event.

3. The Yaracuy Valley: Geological and Tectonic Setting

The Yaracuy Valley is 80 km long and 15 km wide. This valley is bounded by the Sierra de Aroa mountain chain to the NW and the Sierra de Nirgua to the SE (Figure 3). The mountainous reliefs are composed of Paleozoic to Cretaceous age metamorphic rocks (Figure S1 in the supporting information) [*Bushman*, 1959; *Bellizzia and Rodríguez*, 1976; *de Juana et al.*, 1980; *Urbani*, 2008; *Coello*, 2012; *Nevado*, 2012]. The Yaracuy Valley is filled by Quaternary fluvial deposits dipping toward the SW with several fans offset by the Boconó fault [*Coplanarh*, 1975; *Schubert*, 1982; *Casas-Sainz and Diederix*, 1992; *González et al.*, 2008, 2012]. From longitude 69°07′W to 68°42′W the Boconó fault delimits the southeastern flank of the Sierra de Aroa with a

N50–60° direction, and then from longitude 68°42′W to 67°47′W it crosscuts the valley with a N80° direction. From longitude 68°37′W to 68°05′W, the Morón fault delimits the northwestern flank of the Sierra de Nirgua (Figure 3).

Many geologists have mapped the Boconó fault in this valley, and they all reported a predominantly dextral movement and a Quaternary activity suggested by offset alluvial fans. However, they had different interpretations for the dip-slip component of the fault (normal or reverse). *Schubert* [1983] postulated that the slip of the fault is mainly right lateral with a normal component based on the presence of grabens and triangular facets (but the geographical locations for these observations are not given). He proposed that the valley is a pull-apart resulting from the dextral and normal movements of the Boconó and Morón faults. *Casas-Sainz* [1992] proposed that the fault is segmented into two parts, with a significant reverse component. He also assumed that the valley results from the diachronous movement of the two dextral and reverse bordering faults: the Morón fault which was active until the Mio-Pliocene and the Boconó fault which was active during the Quaternary. More recently, *Audemard* [2016] identified three principal segments along the Boconó fault in the Yaracuy Valley (Figure 3), the existence of a reverse component of slip and numerous parallel and truncated traces. The three principal segments are (1) Triste-Albarico segment (N70–N80°) crosscutting the Yaracuy Valley, (2) Albarico-La Virgen segment (N60°) which borders the Sierra de Aroa, and (3) La Virgen-Yaritagua (N60°) segment which also borders the Sierra de Aroa but where the fault trace is more ramified [*Audemard*, 2016]. The lack of morphological expressions in La Virgen justified the distinction between the two last segments (e.g., in Figure S2).

Quaternary offset alluvial fans were used to estimate a slip rate on the Boconó fault in the Yaracuy Valley. However, investigators did not date them with absolute method. *Schubert* [1982] estimated a slip rate of several cm yr^{-1}, *Casas-Sainz* [1991] assessed a slip of $1.3^{+0.8}_{-0.3}$ mm yr^{-1}, and finally *Casas-Sainz* [1995] proposed a rate of 2.6 mm yr^{-1}. In detail, the estimation of *Schubert* [1982] is based on the Yaritagua fan, offset of 1.5–2 km. By proposing a correlation with other dated alluvial fans in the Andes, he assigned to this fan a Late Pleistocene–Holocene age. The assessment of *Casas-Sainz* [1991] ($1.3^{+0.8}_{-0.3}$ mm yr^{-1}) is also based on the Yaritagua fan. He measured an offset of 1250^{+750}_{-250} m. He supposed that the fan was formed during a glacial period at 0.95 Ma. Finally, *Casas-Sainz* [1995] used an alluvial fan near Campo Elias; he determined an offset of 915 m (750 m of horizontal displacement adding a vertical component). He supposed that the fan was formed during a glacial period at 0.35 Ma. Unfortunately, there are no uncertainties reported on the slip rate estimation (2.6 mm yr^{-1}). These known rates are inconsistent among themselves, since these authors did not use dating methods. Therefore, uncertainties based on the deposit ages are not proposed. Our study using absolute dating method will allow us to solve this inconsistency.

Figure 3 shows that numerous other faults crosscut the Yaracuy region: La Victoria-Guacamaya, Socremo, El Guayabo, Aroa, Duaca, and Moron faults. Neotectonic studies reported that the La Victoria-Guacamaya fault is mainly dextral with a Quaternary slip rate of ~0.6 mm yr^{-1} estimated from right-lateral drainage offsets [*Audemard et al*., 2000, and references therein]. The Socremo fault is mainly reverse with a right-lateral component, with an extrapolated slip rate of less than 2 mm yr^{-1} (assessed by paleoseismology) [*Audemard et al*., 2000, and references therein]. The two traces of El Guayabo dextral fault limit a transpressive relief strongly dissected [*Urbani*, 2014; *Baquero et al*., 2015]. Its activity probably stopped after the Mio-Pliocene [*Casas-Sainz*, 1992]. The Aroa fault affects Miocene units [*Coello*, 2012; *Hernandez S*, 2013]. The Duaca fault has Pre-Miocene activity. [*Coello*, 2012; *Hernandez S*, 2013]. Since the Quaternary activity of the Morón fault and Quaternary deformations associated to the Boconó fault are still debated, we remapped faults and morphological markers using several data sets of high-resolution satellite images and aerial photographs.

4. Methods

4.1. Mapping of Faults and Quaternary Morphological Markers

Mapping of markers offset by the fault was carried out using several high-resolution data sets: aerial photographs, satellite optical images, or digital elevation models (DEM). These data sets were combined to detect deformation at different scales [*Zielke et al*., 2015]. We used (1) 1:35 000 aerial photographs, (2) SPOT 4 satellite images on which the pixel size is 20 m, (3) SPOT 5 images on which the pixel size is 5 m, (4) Shuttle Radar Topography Mission digital elevation models on which the pixel size is 30 m spatial resolution, (5) DEMs

Table 1. Description of Each Generation of Alluvial Fans Description Based On Amplitude of Incisions and Geometrical Interrelationships

Generations	Geomorphological Descriptions	Depth of Incisions	Separation Between Incisions	Age
A	Alluvial fans only incised by the active main stream			Younger
B	Alluvial fans incised (but not necessarily over their whole area)	< ~ 4 m < ~ 7 m	~ 100 m ~ 200 m	
C	Alluvial fans incised (but not necessarily over their whole area)	< ~ 10 m ~ 20 m	~ 100 m ~ 500 m	
D	Alluvial fans strongly incised over their whole area	> ~ 10 m	~ 100 m	Older

acquired from the DLR's TanDEM-X satellite (DLR: German Aerospace Center) on which the pixel size is 12 m, and (6) DEMs with 2 m resolution generated from Pleiades stereo images on which the pixel size is 0.50 m (constructed with AMES-StereoPipeline, an open-source software [*Moratto et al.*, 2010]). Comparison of these data sets combined with fieldwork analysis enables us to correlate geomorphic markers on either side of the faults on a larger scale, to determine their geometry before deformation using the method of back slipping restoration at fault scale [e.g., *McGill and Sieh*, 1991; *Klinger et al.*, 2005; *Beauprêtre et al.*, 2012; *Scharer et al.*, 2014; *Rizza et al.*, 2015], and to determine the original shapes of markers before denudation (needed for cosmogenic nuclide dating). We used ArcGis® tools to determine the slope, shape, and surface area of catchment and alluvial fans. We then analyzed the amplitude of incisions and the

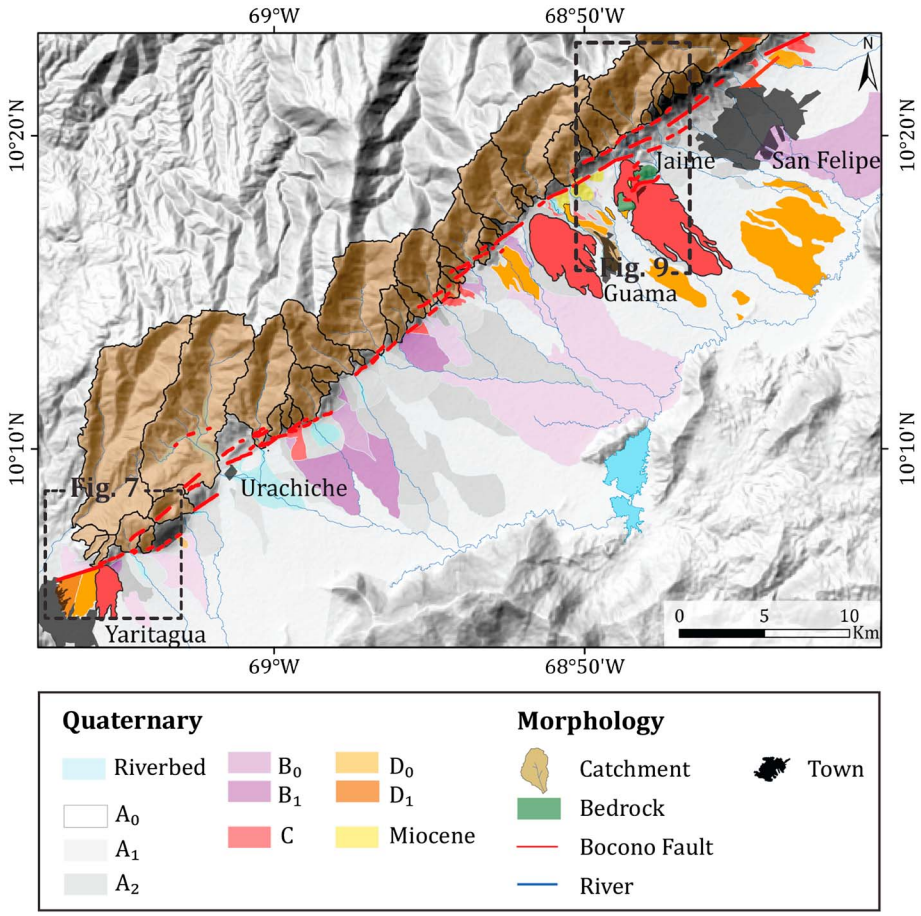

Figure 4. Quaternary mapping of the Yaracuy Valley based on aerial photographs and on a 12 m resolution DEM. The catchments are rotated clockwise, which suggests a significant dextral slip along the fault since the establishment of this catchments system. Emphasized catchments and fans are those clearly offset by the Boconó fault (see restoration of their connection in Figure 6).

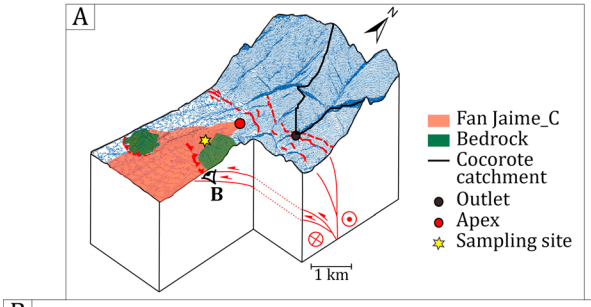

Figure 5. (a) Three-dimensional diagram near Jaime City. The topographic contours were obtained with the DEM constructed with Pleiades images using an ArcGis® tool. Surface mapping was based on field work and analysis of high-resolution images. The fault geometry at depth is an interpretation of these observations. (b) Field photo of the scarp associated to a reverse kinematic. The dashed red line represents the fault trace.

geometrical relationships between fans in order to propose a relative chronology of their formation. We defined four principal generations of alluvial fans: A, B, C, and D (see Table 1 for their descriptions), from youngest to oldest. In addition, where possible, we defined a more accurate relative chronology ranging from 0 (youngest) to 2 (oldest) within fans of the same generation. For instance, in generation A we defined fans A_0, A_1, and A_2.

Uncertainties for back slip reconstructions are determined by the range of plausible offsets for a particular marker. This range mostly depends on the image resolution (± 1 pixel equal to 0.5 m for Pleiades image), the preservation of the marker, and the marker's geometry with respect to the fault zone direction [*Peltzer et al.*, 1988; *Yeats and Prentice*, 1996]. For example, in the case of an alluvial fan offset with respect to the catchment outlet, uncertainty is mainly due to the partial erosion of its apex, which is the best piercing point.

4.2. Cosmogenic ^{10}Be Dating

4.2.1. Sampling Strategy and Production Rate

To date offset alluvial fans, we used in situ terrestrial cosmogenic Beryllium 10 nuclides. This dating method provides an exposure age for Quaternary quartz-rich sediments using the attenuation law of *Lal* [1991].

$$N(x,\varepsilon,t) = \frac{P_n \cdot e^{-\frac{x\rho}{L_n}} \cdot \left(1 - e^{-t\left(\frac{\varepsilon\rho}{L_n}+\lambda\right)}\right)}{\frac{\varepsilon\rho}{L_n}+\lambda} + \frac{P_{\mu\text{slow}} \cdot e^{-\frac{x\rho}{L_{\mu\text{slow}}}} \cdot \left(1 - e^{-t\left(\frac{\varepsilon\rho}{L_{\mu\text{slow}}}+\lambda\right)}\right)}{\frac{\varepsilon\rho}{L_{\mu\text{slow}}}+\lambda} + \frac{P_{\mu\text{fast}} \cdot e^{-\frac{x\rho}{L_{\mu\text{fast}}}} \cdot \left(1 - e^{-t\left(\frac{\varepsilon\rho}{L_{\mu\text{fast}}}+\lambda\right)}\right)}{\frac{\varepsilon\rho}{L_{\mu\text{fast}}}+\lambda} + N_0 \cdot e^{-\lambda \cdot t} \quad (1)$$

where nuclide concentration $N(x,\varepsilon,t)$ (at·g^{-1}) is a function of depth x (cm), denudation rate ε (cm yr^{-1}), and exposure age t (year). P_n, $P_{\mu\text{slow}}$, $P_{\mu\text{fast}}$ (at·g^{-1} yr^{-1}) are production rates of neutrons, slow muons, and fast muons. ρ is the density (g cm^{-3}). L_n, $L_{\mu\text{slow}}$, and $L_{\mu\text{fast}}$ are the attenuation lengths of neutrons, slow muons, and fast muons (160, 1500, and 4500 g cm^{-2}, respectively) [*Heisinger et al.*, 2002a, 2002b]. λ is the radioactive decay constant (4.997×10^{-7} yr^{-1}), and N_0 is the inherited nuclide concentration (at·g^{-1}).

Production rate contributions of slow and fast muons were calculated using the parameters and methods published in *Braucher et al.* [2011]. For the neutronic contribution, we evaluated existing references on spallation production in Low-Latitude High-Altitude sites [*Blard et al.*, 2013; *Kelly et al.*, 2013; *Martin et al.*, 2015] and selected the *Kelly et al.* [2013] production rate assigned by the CRONUS Calculator V2.2 (3.64 ± 0.08 at

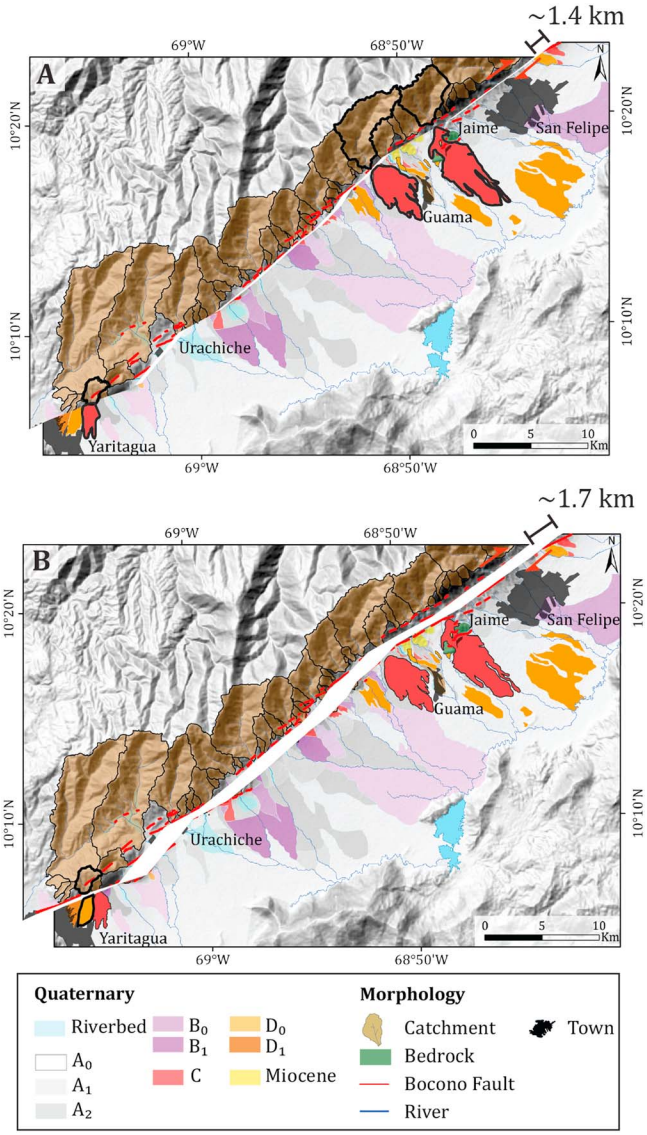

Figure 6. Examples of simple restorations using the geometry shape of each marker and assuming that (1) the apex and outlet can be identified with catchments and alluvial fan shapes and incisions, (2) catchments were originally situated at the east of the fans, and (3) catchments and fans have similar surface areas. In each restoration, we highlighted the reconstructed markers in black. (a) Restoration of Jaime, Guama, and one of the Yaritagua alluvial fan's (filled in red) paleo-positions using an offset of ~1.4 ± 0.2 km. (b) Restoration of paleo-position of another Yaritagua alluvial fan (filled in orange) using an offset of 1.7 to 2.0 km. This restoration is less accurate as the fan is strongly dissected and its apex is probably partly eroded or covered by another deposit.

$^{10}Be{\cdot}g_{quartz}^{-1}$ yr^{-1}) in order to be compatible with other users of CRONUS and because the sampling site is nearest to Venezuela. Finally, we scaled this production for latitude and elevation [*Stone*, 2000].

In equation (1), the unknown parameters are exposure age, denudation rate, and inherited nuclide concentration. Thus, to solve it, we carried out "depth profiles" in order to measure ^{10}Be nuclide concentrations of samples at different depths in the sedimentary deposit (as explained in *Anderson et al.* [1996]).

4.2.2. Depth Profile Simulations

To fit our data to equation (1) and to determine the free parameters (exposure age, inheritance, and denudation), we performed models calculated using the Monte Carlo approach of *Hidy et al.* [2010]. This approach determines the parameters that minimize the difference between the observed and the theoretical ^{10}Be concentration values using the χ^2 test ($\chi^2 = \sum_{i=0}^{n}\left(\frac{C_i - C_{(xi,\varepsilon,t)}}{\sigma_i}\right)\wedge 2$ where C_i is the measured ^{10}Be concentration at depth xi, $C(x_i, \varepsilon, t)$ is the modeled ^{10}Be concentration determined using equation (1), σ_i is the analytical uncertainty at depth i, and n is the total number of samples in the profile). Minimum χ^2 values thus correspond to the best solutions [*Siame et al.*, 2004; *Braucher et al.*, 2009]. However, as proposed by *Ruszkiczay-Rüdiger et al.* [2016] the code was modified in order to take into account the theoretical muogenic production of *Braucher et al.* [2011] and the chosen spallation production rate. For each data set, free parameters were first constrained by thresholds (see section 5), and then we accepted fits that satisfied the condition: $\chi^2_{min} \leq \chi^2 \leq \chi^2_{min} + 1$ [e.g., *Braucher et al.*, 2009; *Delmas et al.*, 2015], which is considered as a substitute of 1σ confidence interval [*Bevington and Robinson*, 2002].

5. Results

5.1. Quaternary Morphotectonic Mapping

We used aerial photographs to study 65 km of the Boconó fault trace in the Yaracuy Valley, in which we identified 18 segments separated by geometric discontinuities (> 100 m), such as overlaps and relay zones. Along

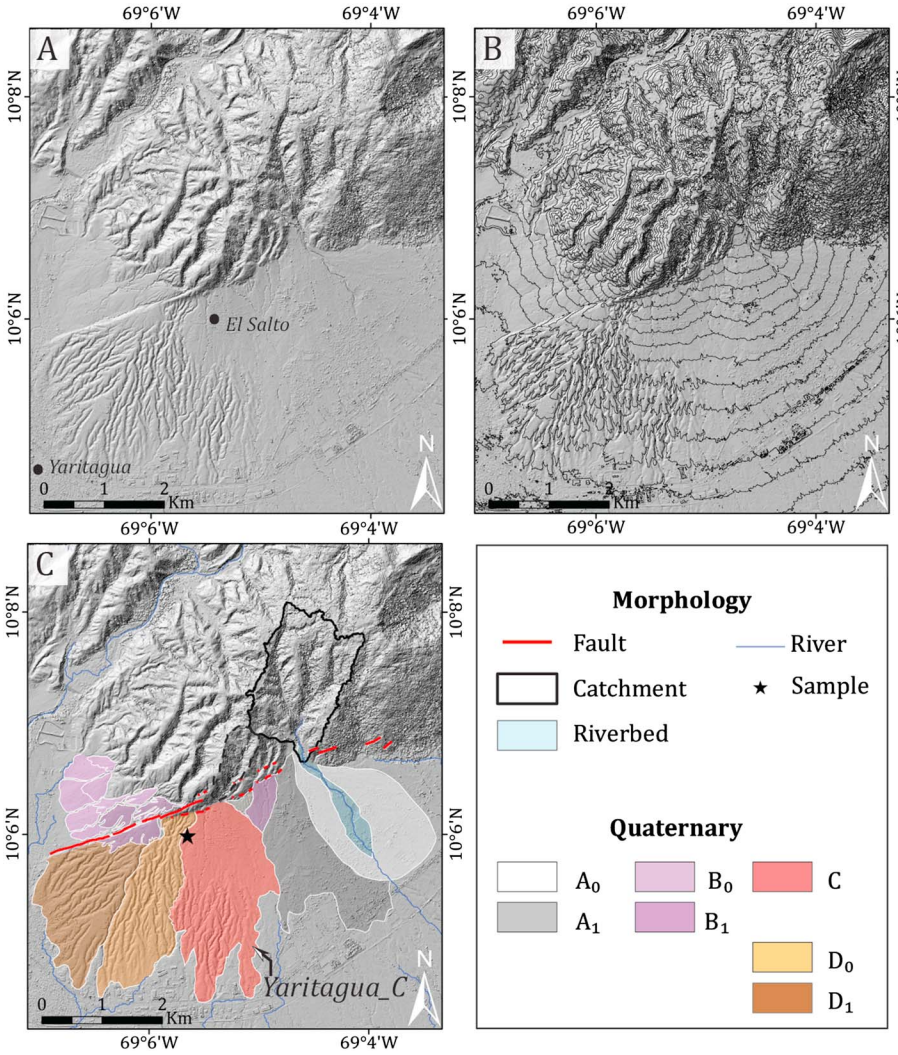

Figure 7. Yaritagua fans. (a) Shaded DEM constructed with high-resolution Pleiades images. (b) Topographic lines with 20 m spacing. (c) Quaternary mapping of alluvial fans and fault traces. The Quebrada de Los Santos catchment is outlined in black continuous line.

these segments—which range in length from 1 to 16 km—we noticed several truncated and parallel traces (Figures S2 and S3). We also observed multiple deformed Quaternary markers showing right-lateral displacement (Figures S2–S4 and 4). In some areas reverse fault segments deformed Quaternary surfaces (for example, Jaime City, see Figure 5). On the scale of the mountain ranges, river catchments in the Sierra de Aroa have been passively rotated clockwise, consistent with a dextral movement along the fault (Figure 4).

Along the Morón fault, we observed triangular facets and tectonic deformation in Miocene units (Urama, Maporita Formations) (Figures S1 and S5). In the Sierra de Nirgua massif, most of the catchments in contact with this fault have an elongated shape perpendicular to the front (up to 25 km long) compared to catchments in Sierra de Aroa (up to 10 km long) (Figure 3). Valleys are relatively wide (up to 1.3 km) compared with valleys in the Sierra de Aroa massif (up to 0.1 km) (Figure 3). At the mountain-piedmont transition zone, river slope is very gentle and vertical incision within the flood plain is low and constant along several kilometers. We also did not observe alluvial fans at the outlets of the catchments.

5.2. Offset Measurements

We found four principal fan generations in the Yaracuy Valley: A, B, C, and D (Table 1). Near the cities of Yaritagua, Guama, and Jaime, fans C and D are disconnected from their respective catchments (Figure 4).

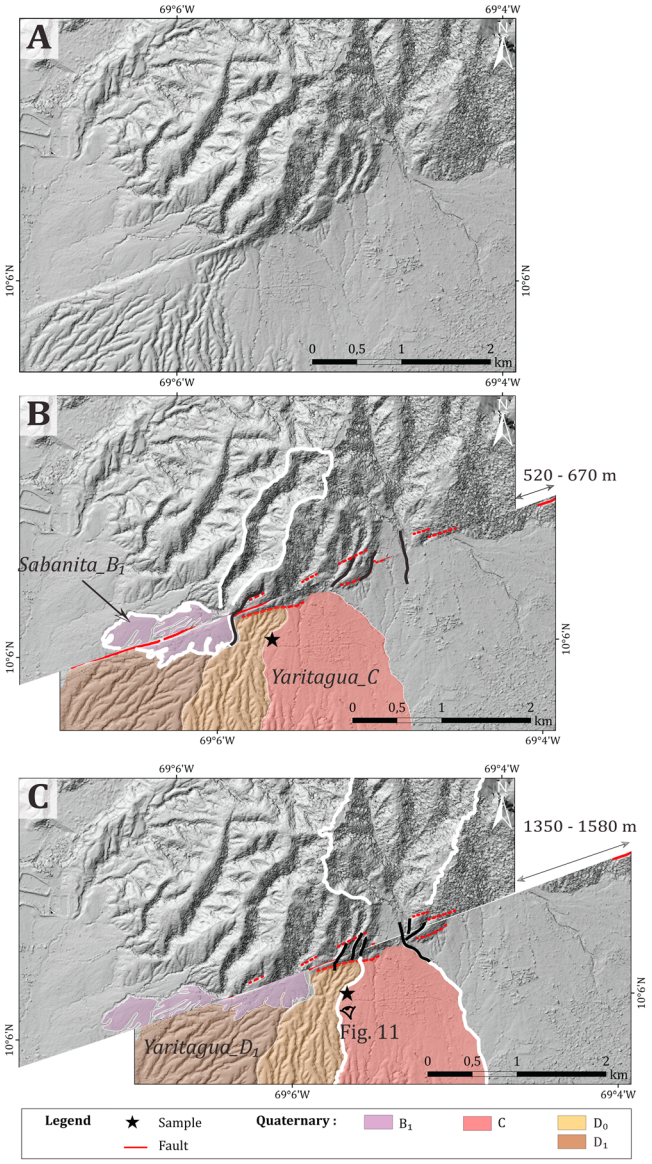

Figure 8. Examples of two back slip reconstructions, with black lines representing morphotectonic markers (e.g., incisions, ridges, or relief that fit between each other after back slip reconstruction). (a) Original image. (b) Restoration of fan Sabanita_B_1 paleo-position with an offset of 520–670 m. (c) Restoration of fan Yaritagua_C paleo-position with an offset of 1350–1580 m. For each back slip reconstruction the fan and the catchment analyzed are outlined in white. See Figure S9 for the minimal and maximal offsets.

At the regional scale, to measure these offsets, we restored the original connections between the fans and their catchments on the 12 m resolution DEM. This simple restoration using the geometry shape of each fan apexes and corresponding outlets allowed us to measure an offset of ~1.4 ± 0.2 km for three fans (Figure 6a). This measurement on three separate and similar markers shows that the offset is reliable and can be used to estimate the fault slip rate. To be more accurate, we restored independently two catchment-fan systems, the Yaritagua and Jaime ones. Especially as these fans are less incised we avoid uncertainties on back slip reconstruction and on surface exposure dating. Uncertainties for back slip reconstructions are determined by the range of plausible offsets for a particular marker. In our cases of study this range mostly depends on the image resolution (± 2 m for our satellite images), the preservation of the marker, and the vegetation which is intense in our area.

5.2.1. Yaritagua Alluvial Fans

Distribution of the faulting. Between the cities of El Salto and Yaritagua, in the alluvial plain, we observed a 2 km long scarp oriented N70° (Figures 7 and S6). The scarp decreases progressively in height from 2 to 3 m at El Salto to Yaritagua where it disappears. Two drainages on the southern flank of the scarp seems to be beheaded (Figure S6) as they incise 6–8 m of the main scarp and as they can be restored (see Figure 8), and this suggest that the scarp origin is due to tectonic.

Fan characteristics and offset measurements. Four generations of fans were identified within the piedmont: some fans characterized by a lack of or relatively small offsetting (Yaritagua_A and Yaritagua _A_1) and other fans disconnected from their original catchment (Yaritagua _C and Yaritagua _D fans). *Dade and Verdeyen* [2007] relation states that a fan and its respective catchment should have similar areas.

Fan Yaritagua_A: This relation is satisfied for the *Quebrada de Los Santos* catchment (~2.9 km^2) and the fan Yaritagua_A (~3.1 km^2) which is still active and is not offset by the fault.

Fan Yaritagua_A_1: The *Dade and Verdeyen* [2007] relation is also satisfied for the same catchment (~2.9 km^2) and the fan Yaritagua _A_1 (~2.6 km^2). This fan is offset by less than 120 m.

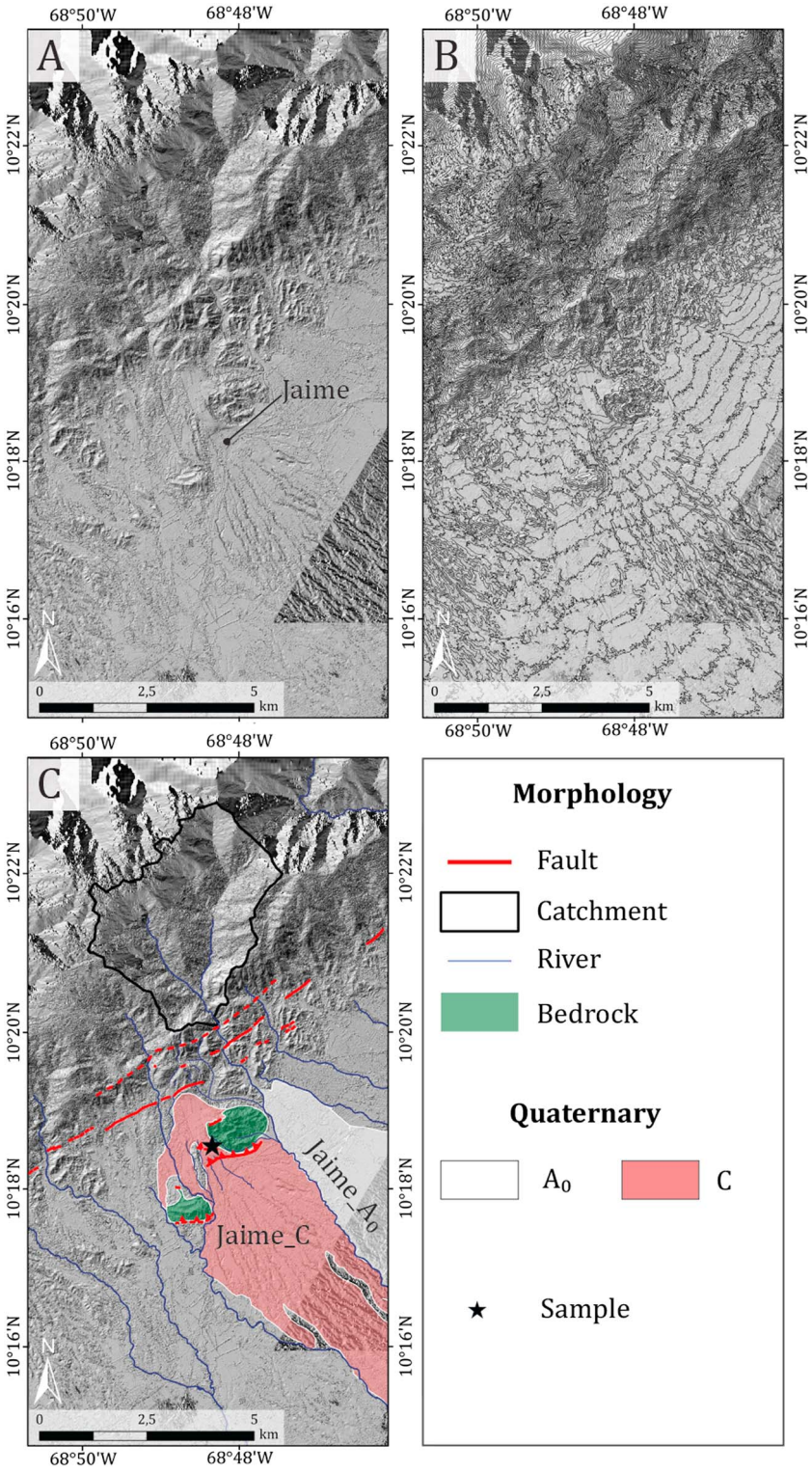

Figure 9. Jaime fans. (a) Shaded DEM constructed with Pleiades images (light gray) and shaded DEM of 12 m resolution (dark gray). (b) Topographic lines at 20 m intervals. (c) Quaternary mapping of alluvial fans and fault traces. The Cocorote catchment is outlined in black.

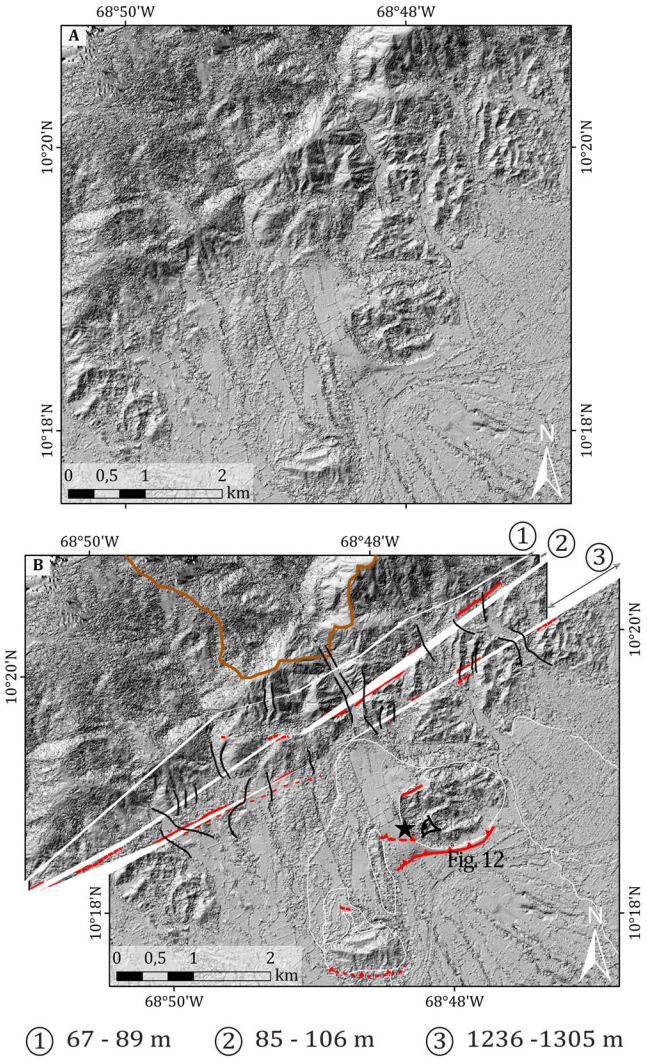

Figure 10. (b) Original image. (b) Back slip reconstruction of the alluvial fan Jaime_C. The brown line emphasize the Cocorote catchment. Black lines represent morphotectonic markers (incisions, ridges, or relief that fit between each other after back slip reconstruction), and red lines represent active faults with movement indicators. Offset 3 is measured on the fault trace separating the apex and the outlet, and it gives the minimum lateral displacement. Offsets 1 and 2 are measured on other parallel traces that may have been active after the fan deposition, in which case reconstructions give a maximum lateral displacement. See Figure S10 for the minimal and maximal offsets.

Fan Yaritagua_C: Its area is ~3.7 km^2 which is comparable to the *Quebrada de Los Santos* catchment area (~2.9 km^2). This fan is also issued from this catchment, as shown in Figure 4. One also may argue that the Yaritagua_C fan is in reality composed of two geomorphic surfaces: an incised fan in the distal area which is in part buried by a second younger fan poorly incised. Under this assumption these two fans cannot come from the same catchment. The older fan was probably connected to the *Quebrada de Los Santos* catchment, and the younger fan was connected thus to a smaller catchment. However, the younger fan's area is 1.5 km^2 whereas the hypothetic associated catchment area is 0.5 km^2, this is in contradiction with the *Dade and Verdeyen* [2007] relation. In addition, we performed several topographic profiles showing that there is no discontinuity of slope along the incised (lower) part and the flat (upper) part of the fan (Figures S7 an S8). Therefore, we interpret this morphology as that of a single fan undergoing retrogressive erosion. To enhance the offset measurements, we used back slip restoration on high-resolution Pleiades images of (i) alluvial fan and its catchment and (ii) drainages and ridges. These reconstructions allows us to estimate an offset of 1.36 to 1.58 km for the fan Yaritagua_C (Figure 8b).

Fan Yaritagua_D_0 and Yaritagua_D_1: The fans have a similar area (~2.3 and ~2.7 km^2, respectively) which are comparable to the *Quebrada de Los Santos* catchment area (~2.9 km^2). These fans are thus also probably issued from this catchment (Figure 4). For the fan Yaritagua _D_0 we measured an offset ranging from 1.7 to 2.0 km (Figure 6b).

Fan Sabanita_B_1: This fan derives from a smaller catchment (located to the west of the Quebrada de Los Santos catchment). It is cut by the fault along its longitudinal direction. Back slip reconstruction to connect the two parts separated by the fault shows that the fan Sabanita_B_1 is offset by 520 to 670 m (Figure 8b).

5.2.2. Jaime Alluvial Fans

Near Jaime, the Boconó fault is segmented into several parallel and truncated segments. Within uncertainties due to the vegetation cover, we mapped three parallel traces crosscutting the relief and a main reverse fault within the piedmont (Figures 5 and 9). We also mapped an alluvial fan which is highly dissected in its downstream part and disconnected from the Cocorote catchment outlet (Jaime_C in Figure 9). The area of the fan

Table 2. Local Surface Production Rates by Spallation, Slow Muon Capture and Fast Muon Radiation (at·g^{-1} yr^{-1}) for Each Sampling Site

Sampling Site	Latitude	Longitude	Altitude	Pressure[a]	Shielding Factor[b]	Production Rate		
	(°N)	(°W)	(m)	(hPa)		(atoms·g^{-1} yr^{-1})		
						Spallation	Fast Muons	Slow Muons
Fan Yaritagua (Ya_C)	10.09997	69.09438	525	952.42	0.999397846	3.43	0.044	0.015
Fan Jaime (Ja_C)	10. 3094	68.8057	563	948.32	0.999	3.53	0.044	0.015

[a]Pressure has been estimated using the offline MATLAB code CRONUS calculator (NCEPatm_2.m).
[b]Shielding scaling factors have been calculated following *Dunne et al.* [1999] method.

(~14.2 km^2) is slightly less than that of the catchment area (~18.7 km^2), but they are of the same order of magnitude. Back slip reconstructions on high-resolution Pleiades images allows us to connect the alluvial fan apex to the outlet of the catchment (Figure 10). Considering only the offset on the trace separating the apex and the outlet (offset 3 in Figure 10), the reconstruction yields a minimum offset of 1236 m.

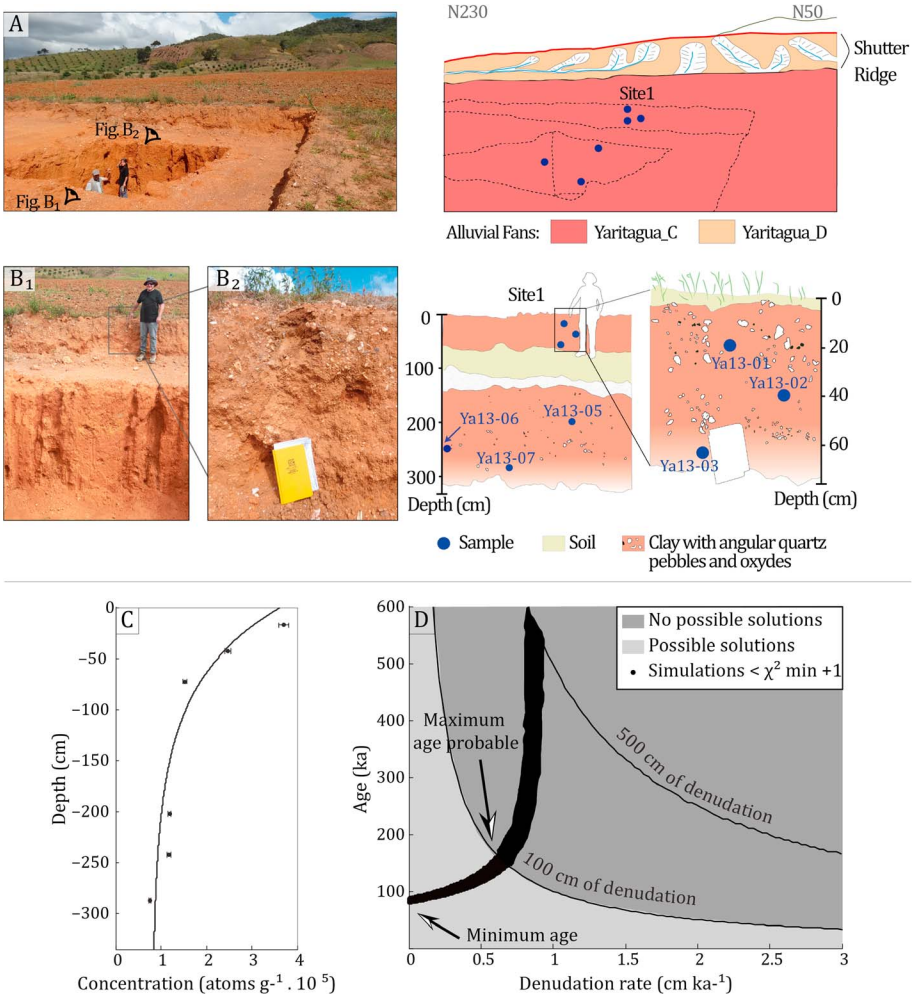

Figure 11. Photos of the sampling site (in fan Yaritagua_C) (see in Figure 8 location of the view direction). (a) Sample site location. (b) The sedimentary deposit from which the six quartz cobbles were sampled. Results of the depth profile simulations for the fan Yaritagua_C using the Monte Carlo approach of *Hidy et al.* [2010] modified by *Ruszkiczay-Rüdiger et al.* [2016] (see method 4.2.2). (c) Concentration versus depth plot showing the best fit depth profile for equation (1) using our sample concentrations (black dots). (d) Exposure age-denudation rate plot for the simulations using the parameters in Table 4. The solid and dashed black curves mark 100 and 500 cm of total denudation, respectively.

Table 3. Beryllium 10 Data for the Yaritagua Site[a]

Samples	Depth	Quartz[b]	^{9}Be Carrier	^{10}Be/^{9}Be[c]		^{10}Be Concentration	
				Value	Uncertainty	Value	Uncertainty[d]
	(cm)	(g)	(mg)	($\times 10^{-13}$)	(%)	($\times 10^{3}$ at·g_{quartz}^{-1})	
Yaritagua: Quartz Cobbles							
YA13-1	15	18.79	0.3001	3.491	3.27	370	12.1
YA13-2	40	17.18	0.3002	2.141	3.29	247	8.2
YA13-3	70	18.45	0.2999	1.423	5.25	152	8.0
YA13-5	200	15.02	0.3008	0.9139	9.57	119	11.4
YA13-6	240	17.94	0.3005	1.075	5.41	118	6.4
YA13-7	285	19.16	0.3007	0.758	6.37	77	4.9

[a]Results have been corrected according to the chemical blank (^{10}Be/^{9}Be blank = 2.63844 × 10–^{15} with 33.72% of uncertainty). Beryllium 10 concentrations were calibrated against National Institute of standard and technology (NIST) standard reference material 4325 using a ^{10}Be/^{9}Be ratio of (2.79 ± 0.03) × 10^{-11} [*Nishiizumi et al.*, 2007].
[b]Chemical extraction was performed in the cosmogenic ISTerre Laboratory (Grenoble, France) following procedures adapted from *Brown et al.* [1991] and *Merchel and Herpers* [1999]. The ^{10}Be half-life used is (1.387 ± 0.012) × 10^{6} years [*Chmeleff et al.*, 2010; *Korschinek et al.*, 2010].
[c]To estimate analytical uncertainty propagations, we used the methods of *Davis et al.* [1999] and *Gosse and Phillips* [2001].
[d]Measured at the French National AMS facility (accelerator mass spectrometry) in ASTER located in CEREGE, Aix-en-Provence [*Arnold et al.*, 2010].

However, the other parallel traces may have been active after the fan deposition, in which case the reconstructions imply a maximum lateral displacement of 1500 m.

5.3. Exposure Age Determinations

To estimate slip rates, we chose to date the abandonment of fan Yaritagua_C and fan Jaime_C (Table 2), offset by 1350–1580 m and 1236–1500 m, respectively.

5.3.1. Fan Yaritagua_C

At the sampling site (black star in Figure 8), we observed one sedimentary unit in the deposit composed of unbedded sparse quartz clasts in a lateritic matrix (Figure 11). We carried out a "depth profile" using individual clasts of quartz (no other suitable materials were available for dating). We collected six samples from 15 to 285 cm depth (Table 3).

Depth profile simulations were performed to estimate an exposure age (see section 4.2.2). To constrain the simulations, we first supposed a density ranging from 1.8 to 2.2 g cm^{-3} as the deposit is mainly composed of clay [*Veihmeyer and Hendrickson*, 1948]. We had no prior assumptions with respect to the denudation rate and to the total denudation; however, we must define a range for the simulation. Therefore, it was constrained, respectively, between 0 and 5 cm ka^{-1} and between 0 and 5 m. The maximum values are overestimated considering the flat and poorly incised surface sampled (Figures 8 and 11b). The minimal χ^2 obtained was 62.4; therefore, we chose a χ^2 cutoff of 63.4 (χ^2_{min} + 1) and calculated 100,000 models (Table 4).

The Monte Carlo approach of *Hidy et al.* [2010] yields a minimum exposure age of 79 ka and then a trade-off where several simulations reach a steady state (Figures 11c and 11d). In this case we can only determine a

Table 4. Parameters Used in the Monte Carlo Search Routine of *Hidy et al.* [2010] to Determine the Exposure Age of Fan Yaritagua_C and Fan Jaime_C

	Fan Yaritagua _C		Fan Jaime _C	
Thresholds	Min	Max	Min	Max
Denudation rate (cm ka^{-1})	0	5	0	5
Total denudation (cm)	0	500	0	500
Age (ka)	0	600	0	500
Inheritance (10^{3} at·g^{-1})	0	200	0	200
Density	1.8	2.2	2	2.4
χ^2 cutoff = χ^2_{min} + 1	62.4	63.4	431.8	432.8

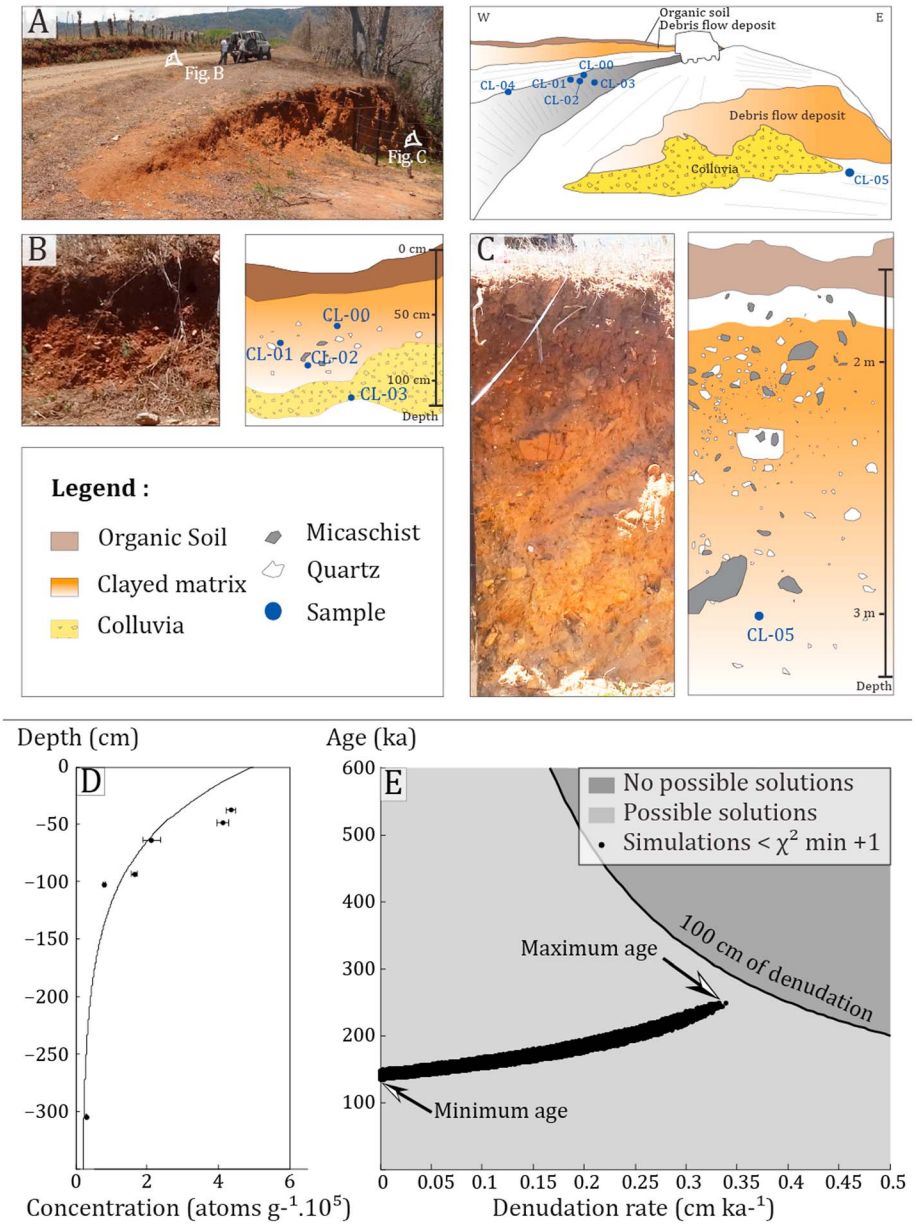

Figure 12. (a–c) Location of the sample site within the alluvial fan Jaime_C (see Figure 10 for the site location). The deposit is composed of quartz cobbles and mica schist clasts in a clayey matrix, in which there is no graded bedding or stratification. (d and e) Same as in Figures 11c and 11d but for the fan Jaime_C.

minimum exposure age, considering no denudation, which is 79 ka. Therefore, it implies a slip rate < 20.0 mm yr^{-1}.

5.3.2. Fan Jaime_C

We sampled the alluvial fan on a preserved surface (not influenced by gully's incisions) and far from urbanized zones (Figure 10). The sampled deposit is composed of unbedded quartz cobbles and mica schist clasts in a clayey matrix. There is no evidence of interposed deposits within the depth profile chosen for the sampling (Figure 12). To be consistent with the Yaritagua sampling, we only selected quartz cobbles. Six samples were collected from 35 to 300 cm depth (Table 5).

We performed depth profile simulations with the free parameters constrained by reliable values (see Table 4). Density was constrained to a range from 2 to 2.4 g cm^{-3} as the deposit is mainly constituted of pebbles

Table 5. Beryllium 10 Data for the Jaime Site[a]

Samples	Depth	Quartz[b]	^{9}Be Carrier	^{10}Be/^{9}Be[c]		^{10}Be Concentration	
				Value	Uncertainty	Value	Uncertainty[d]
	(cm)	(g)	(mg)	($\times 10^{-13}$)	(%)	($\times 10^{3}$ at·g_{quartz}^{-1})	
Jaime: Quartz Cobbles							
CL-00	35	20.7911	0.3034	4.505	3.06	438	13.4
CL-01	45	20.2651	0.3042	4.149	3.38	414	14.1
CL-02	60	19.5066	0.3004	2.092	11.69	213	24.9
CL-03	90	24.2031	0.3049	1.964	4.67	165	7.6
CL-04	100	19.2094	0.3021	0.794	3.84	81	3.1
CL-05	300	19.9221	0.3038	0.323	6.06	31	1.9

[a]Results have been corrected according to the chemical blank (^{10}Be/^{9}Be blank = 2.63844 × 10–15 with 19.31% of uncertainty). Beryllium 10 concentrations were calibrated against the ASTER standard (STD11) with a ^{10}Be/^{9}Be ratio of (1.191 ± 0.013) × 10–^{11} [*Braucher et al.*, 2015].
[b]See Table 3.
[c]See Table 3.
[d]See Table 3.

(Figure 12). Age, inheritance, and denudation were constrained as for simulation of the fan Yaritagua_C. The minimal χ^2 is 431.8, so we chose a χ^2 cutoff of 432.4. Based on these assumptions, the Monte Carlo approach determines a range of ages between 134 and 248 ka (solutions contained within the [min χ^2_{min}; χ^2_{min} + 1] bracket) (Figures 12d and 12e). This yields a slip rate of 5.0–11.2 mm yr^{-1}.

5.3.3. Uncertainties on Exposure Ages

Exposure ages were determined by minimizing the difference between the observed and the theoretical ^{10}Be concentration values (χ^2 test) (see section 4.2.2). The minimum χ^2 values used in our simulations (χ^2_{min} ~ 60–432) are relatively high values that are due to the scattering of the concentrations with respect to the theoretical model. This scattering is probably explained by different inheritance in each sample, and, as we sampled one quartz cobble at each depth (no other suitable materials were available for dating), this effect is probably amplified.

5.4. Homogenization of Beryllium 10 Dates

To assess a slip rate in the Central Venezuelan Andes between the Boc-b and Boc-c Boconó sections, *Wesnousky et al.* [2012] and *Carcaillet et al.* [2013] sampled moraines offset by the fault (La Victoria and Los Zerpa moraines in Figure S11). They sampled several boulders on the surface of both moraines and measured their ^{10}Be concentration. In order to compare it with our results, we reevaluate the exposure ages of all samples using the same production rate determined for low latitudes and new muogenic production rates (see section 4.2.1 and Table S1). Concerning moraine TCN dating, in a population of ages, the estimation of the true age is matter of debate. *Putkonen and Swanson* [2003] explain that the oldest date represents the true age arguing that the prior exposure is rare. However, several authors choose to take into account the arithmetic mean [e.g., *Wesnousky et al.*, 2012] or the peak of the summed probability function [e.g., *Carcaillet et al.*, 2013]. In this paper, we will use the arithmetic mean for the following reasons: (1) there is few samples by site and (2) the dates obtained are generally clustered (Figure S11).

On the La Victoria moraine crests, *Audemard et al.* [1999] reported an offset of maximum 100 m. Considering the recalculated exposure ages, we chose a significant exposure age of 18.7 ± 4.3 ka (n = 4) (arithmetic mean). Based on these assumptions the reevaluated maximum slip rate is between 4.3 and 7.0 mm yr^{-1} (published age is 16.5 ± 4.0 ka in *Wesnousky et al.* [2012] which yielded a maximum slip rate of 4.8–8 mm yr^{-1}).

On Los Zerpa moraine crests, *Audemard et al.* [1999] evaluated an offset of 60–100 m. Using the ^{10}Be concentrations measured by *Wesnousky et al.* [2012] and *Carcaillet et al.* [2013], we reevaluated the exposure ages. We determine an exposure age of 18.1 ± 3.3 ka (n = 6), which yields a slip rate ranging from 2.8 to 6.7 mm yr^{-1} (the arithmetic mean of all published ages in *Wesnousky et al.* [2012] and in *Carcaillet et al.* [2013] is 15.6 ± 2.8 ka which yielded a slip rate of 3.2–7.8 mm yr^{-1}).

6. Discussion

6.1. Distribution of the Deformation in the Yaracuy Valley

6.1.1. Quaternary Activity of the Boconó and the Morón Faults

Morphotectonics analysis on the Boconó fault geometry, segmentation, and geomorphology allows us to identify 18 segments as well as several and truncated parallel traces (Figures S2 and S3). This puts in evidence a fault immaturity [*Manighetti et al*., 2015; *Ansberque et al*., 2016]. The passive clockwise rotation of catchments in the Sierra de Aroa is similar to catchment geometries (in terms of topographic elevation and rotation) along the right strike-slip faults of the Southern Alps in New Zealand, modeled by *Castelltort et al*. [2012]. In addition, we observed multiple Quaternary deformation markers and reverse fault segments along the fault. This suggests that the fault has been active during the Quaternary, with mainly dextral kinematics and a minor compressive component.

Along the Morón fault, observation of triangular facets and analysis of the catchment's and valley's geometries suggest an extensional setting. This setting and the presence of deformation in Miocene units suggest that during the Miocene the Morón fault was active and mainly normal. During the Quaternary, erosion and sedimentation processes hid any tectonic evidence. Conversely, along the Boconó fault in the same climatic and lithological contexts there are numerous deformed markers (e.g., scarp within alluvial surfaces and offset fans). If we suppose that the human activities did not hide tectonic evidence, we can therefore infer that active deformation along the Morón fault is either absent or negligible compared to the Boconó fault.

6.1.2. Off-Fault Deformations

With respect to the offset estimations, several coseismic measurements have demonstrated that part of the strain energy can be released by off-fault deformations [e.g., *Rockwell et al*., 2002; *Gold et al*., 2015]. Studies on several faults and laboratory morphotectonic experiments showed that the total displacement accounted by off-fault displacement can range from 0 to 45% [e.g., *Shelef and Oskin*, 2010; *Rockwell and Klinger*, 2013; *Zinke et al*., 2014; *Graveleau et al*., 2015]. Thus, some Quaternary slip rate measurements are probably underestimated. To avoid this, our markers (catchments and fans) cover the whole fault zone, and they are offset by ~1.4 ± 0.2 km, as measured on separate and similar markers. In comparison with other slip rate estimations along the Boconó fault (see section 6.3), we can postulate that our markers are those that record the slip within the larger fault zone along the Boconó fault.

However, the catchment are all rotated, this rotation can suggest an off-fault deformation within the catchments. Numerical modeling could be performed to determine if rivers are passive features and recorded a large-scale tectonic activity [e.g., *Castelltort et al*., 2012].

6.1.3. Comparison Between Regional Geodetic Data and Pleistocene Slip Rates

To investigate the distribution of the deformation in the Yaracuy Valley, we compare the most probable fault slip rate along the Boconó fault with the regional geodetic velocities.

Previous studies along the segment Boc-e of *Schubert* [1982], *Casas-Sainz* [1991] and *Casas-Sainz* [1995] estimated without absolute dating slip rates, respectively, of several cm yr^{-1}, $1.3^{+0.8}_{-0.3}$ mm yr^{-1} and 2.6 mm yr^{-1}. In comparison our study gives a fault slip rate based on absolute dating method and on high-resolution images. This methodology yields a probable right-lateral slip rate of 5.0–11.2 mm yr^{-1} and $<$20 mm yr^{-1}. Our two slip rates are consistent within each other and integrate dating uncertainties unlike previous studies.

GPS studies show an ENE movement of the Maracaibo Block at a velocity of ~9–13 mm yr^{-1} (direction N60°) and a compression rate at ~2–4 mm yr^{-1} (direction N330°) with respect to the stable South American plate [*Pérez et al*., 2011; *Reinoza*, 2014] (e.g., Figure 2b). Assuming the following points (1) the long-term slip rate along the Boconó fault represents 40 to 100% of the ENE geodetic rate, (2) the Boconó fault is mainly dextral with a minor compressive component, (3) active deformation along the Morón fault is either absent or negligible compared to the Boconó fault, and (4) neotectonic studies imply $<$2 mm yr^{-1} of slip rate for the other faults (see section 3), we can postulate that the Boconó fault accommodates 40 to 100% of the deformation in the Yaracuy Valley between the North Andean Block and the South American plate.

This postulation is however based on the geodetic measurements which are scattered in this region [*Pérez et al*., 2011; *Reinoza*, 2014]. Therefore, it is highly recommended to densify geodetic measurements for future studies in order to propose a more specific and accurate percentage.

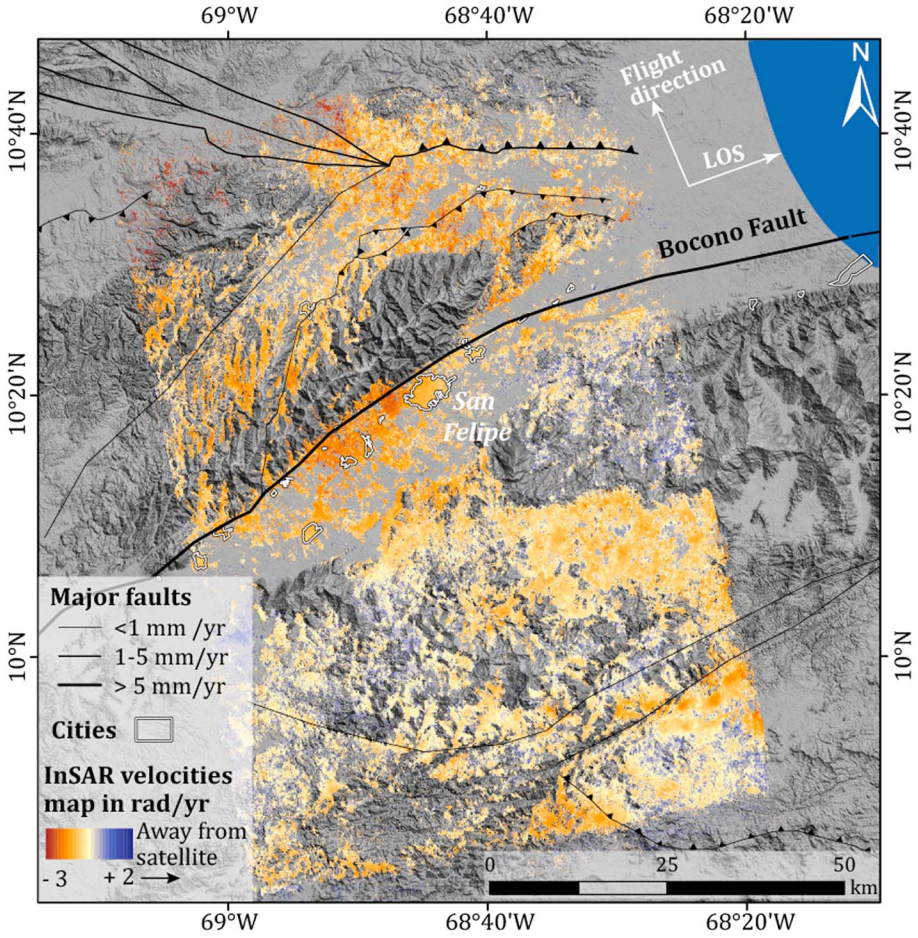

Figure 13. The 45 m resolution InSAR line-of-sight velocity map estimated over a 3.5 year period (2007–2011). This map results from the processing of ascending track A133 (ALOS-1). Positive velocities are oriented away from the satellite whereas negative velocities are oriented toward the satellite. RMS values map for each pixel, estimated over 3.5 years, is shown in Figure S12. ALOS-1 data were obtained from Japan Space Systems © METI and JAXA.

6.2. Slip Deficit Along the Boconó Fault in the Yaracuy Valley

The last historical event in the Yaracuy Valley was the 1812 event [e.g., *Altez*, 2006; *Audemard*, 2016]. *Choy et al.* [2010] assigned a M_{WI} of 7.4 and a rupture length between 90 and 100 km to this earthquake. Slip deficit estimation has to take potential aseismic slip into consideration, by which strain is progressively released into the seismogenic layer [*Ryder and Bürgmann*, 2008; *Shirzaei et al.*, 2013]. As GNSS (Global Navigation Satellite System) data are sparse in time and space in this area and give only a rough estimation of the present deformation (Figure 2b), we performed an InSAR analysis of the Yaracuy region using 16 synthetic aperture radar (SAR) images spanning the 2007–2011 period.

These SAR images from the L band ALOS1 satellite were processed following the same methodology of *Pousse Beltran et al.* [2016] (see Text S1 for detailed method) with the NSBAS (New Small BASeline) method [*Doin et al.*, 2011]. Despite the lack of data in several areas, in the obtained velocity map (Figure 13), there are some localized area of subsidence deformation patterns near the cities (e.g., at the west of San Felipe), this could be due to groundwater pumping. However, absence of high-velocity jump crossing the Boconó fault implies the lack of aseismic slip during the spanned period. If we extrapolate this locked behavior to the last 204 years, and if we consider that our estimated Quaternary slip rate (5–20 mm yr^{-1}) corresponds to the present-day slip rate, by multiplying this rate by the elapsed time locked we obtain a slip deficit of 1 to 4 m. Using the regression for strike slip faults of *Wells and Coppersmith* [1994], this slip deficit corresponds to a M_w 7.0–7.6 earthquake. This magnitude is

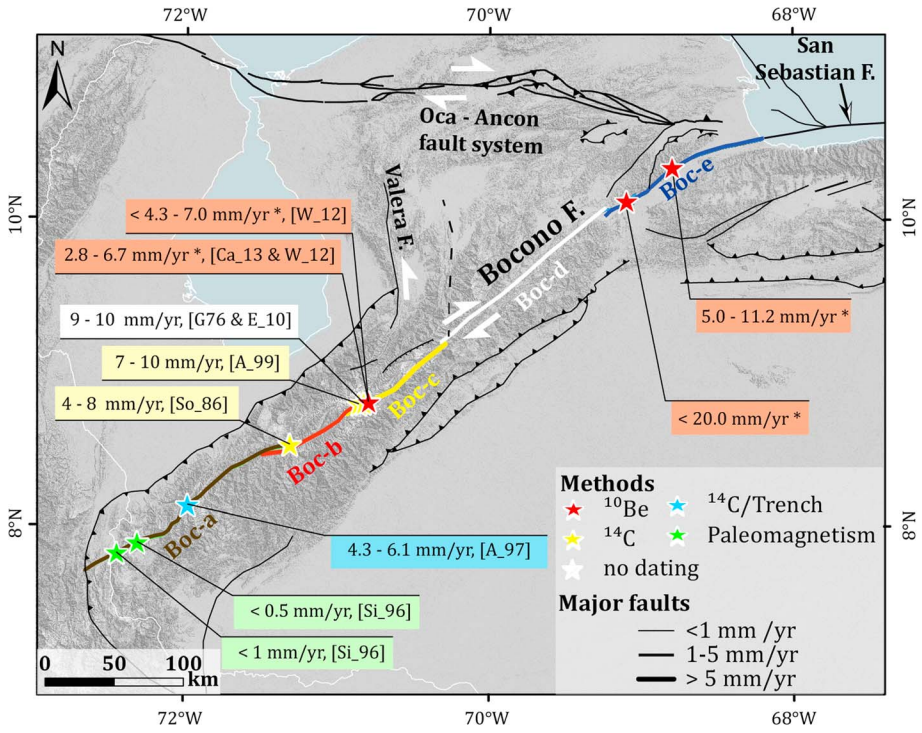

Figure 14. Published and/or modified geological slip rates along the Boconó fault, colored lines highlight the five segments of the fault based on *Audemard et al.* [2000]. Slip rate references quoted are *Giegengack et al.* [1976], *Soulas* [1986], *Singer and Beltan* [1996], *Audemard* [1997], *Audemard et al.* [1999, 2000], *Egbue and Kellogg* [2010], *Wesnousky et al.* [2012], and *Carcaillet et al.* [2013]. Slip rates with an asterisk are those modified or estimated in this work.

comparable to the 1812 earthquake and to the other historical events along the Boconó fault. However, to better assess the seismic hazard along this fault segment, a complete paleoseismic calendar is needed [*Audemard*, 2016]. Moreover, other faults with slower loading rates (e.g., La Victoria Guacamaya fault) should also be studied in detail as this kind of faults can trigger unpredictable and destructive seismic events [*Newman et al.*, 1999; *Gupta et al.*, 2001; *Yano et al.*, 2014].

6.3. Boconó Fault Behavior and North Andean Block Tectonic Setting

Figure 14 summarizes Quaternary slip rate estimations along the Boconó fault. Four of them are based on $<$20 ka offset moraines dated by ^{14}C [*Salgado-Labouriau et al.*, 1977; *Soulas*, 1986; *Audemard et al.*, 1999] or ^{10}Be (recalculated from *Wesnousky et al.* [2012] and *Carcaillet et al.* [2013]). A fifth slip rate has been estimated in a paleoseismologic trench [*Audemard*, 1997]. Other investigations have also proposed slip rates along the fault but without absolute dating methods [*Giegengack et al.*, 1976; *Schubert*, 1982; *Casas-Sainz*, 1995; *Singer and Beltran*, 1996; *Egbue and Kellogg*, 2010].

Unfortunately, based on these large uncertainties and poorly constrained slip rates, it is difficult to discuss a possible slip-rate decrease or a temporally different rate. A remaining option to discuss it is to choose from our results a "preferred" rate. To choose it, we consider that the fault slip rate of the two sites is similar. This is reliable as the two fault traces have a similar strike (70° and 64°) and there is no parallel traces observed; therefore, the Boc-e slip rate should range from 5.0 to 11.2 mm yr^{-1}. In addition, we can propose a maximum age probable for the Yaritagua_C fan based on the maximum denudation possible. According to field observations, the surface fan is flat and not incised; therefore, we can consider that the fan undergone reasonably less than 1 m of total denudation. This is consistent with the maximum total denudation simulated with the Jaime depth profile (Figures 12d–12e). Indeed, the denudation of these two fans should be similar as these two fans have similar morphology, slope, and undergo the same climate. By setting this constrain in our depth profile simulations (Figure 11d) a maximum age of 161 ka can be determined. Considering

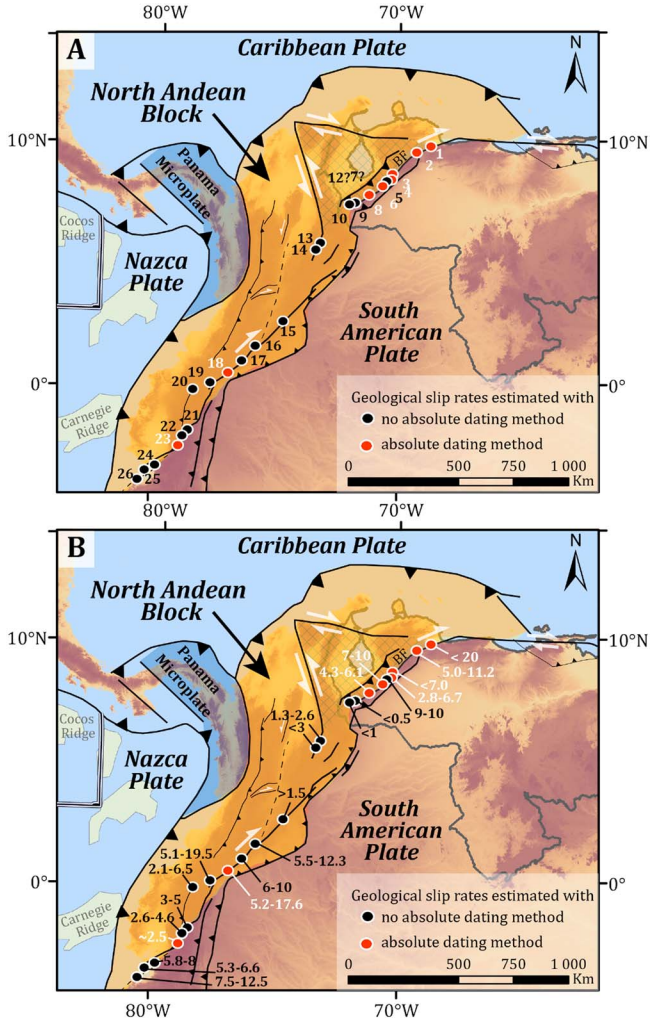

Figure 15. Structural map of the North Andes based on *Egbue and Kellogg* [2010]. Dots represent lateral slip rates estimated along individual faults. (a) Numbers associated with dots correspond to the numbering in Table S2. (b) Same figure with slip rates values displayed.

the measured offset of 1350–1580 m, it yields a minimum slip rate of 8.4 mm yr^{-1}. Therefore, we can propose that our preferred slip rate for the Boc-e segment ranges from 8.4 to 11.2 mm yr^{-1}.

By comparing our preferred slip rate with the slip rates estimated in the Venezuelan Andes on <20 ka markers (Figure 14), our rate is slightly higher. The two exceptions are for the rate estimated without an absolute dating method of *Egbue and Kellogg* [2010] (9–10 mm yr^{-1}) and for the rate of *Audemard et al.* [1999] (7–10 mm yr^{-1}). A lower slip rate measured on <20 ka markers can be explained by two main hypotheses: (1) the slip rate decrease between ~100 and ~20 ka and (2) the difference in marker geometries with respect to the width of the deformation; in the Andes part of the deformation lies outside the area covered by the sampled markers, whereas in the Yaracuy Valley the markers given their position and geometry with respect to the fault zone recorded the totality of the slip.

In the North Andean Block, compilation of the published right-lateral slip rates along the individual faults shows that we are the first to have accurately dated offset markers which are this old (Table S2). Without absolute dating method several study managed to propose slip rate on several hundreds of thousands years [e.g., *Winter et al.*, 1993; *Chorowicz et al.*, 1996; *Dumont et al.*, 2005; *Tibaldi et al.*, 2007; *Witt and Bourgois*, 2010]. Right-lateral slip rates estimated in our study are among the higher slip rates obtained for the North Andean Block. The other high slip rates were estimated (1) in the South of Colombia along the Cayambe fault (dot 16 in Figure 15) by *Tibaldi et al.* [2007] (5.5–12.3 mm yr^{-1}) but without absolute dating and by *Ego et al.* [1996] (5.2–17.6 mm yr^{-1}) (dot 18 in Figure 15) and (2) along the CASF (Cayambe Afiladores Sibundoy fault) in Ecuador (dot 19 in Figure 15) by *Tibaldi et al.* [2007] without absolute dating (5.1–19.5 mm yr^{-1}). Geodetic studies within the North Andean Block estimated a NE escape with respect to the South American plate at a rate of 6–14 mm yr^{-1} [*Pérez et al.*, 2011; *Alvarado*, 2012; *Reinoza*, 2014; *Symithe et al.*, 2015; *Alvarado et al.*, 2016; *Mora-Páez et al.*, 2016]. However, as uncertainties of Quaternary slip rates are wide and as geodetic data are sparse, it only can be stated that the North Andean Block escape is localized along the main dextral faults and remains constant at first order since Middle Pleistocene until nowadays. The North Andean Block is at a first-order stable and homogenous bloc since Middle Pleistocene. It is thus highly recommended to perform block model for the whole North Andean Block using available geodetic data. This is in order to detect relative motions between minor blocks and discuss about the processes driving the NE escape (Carnegie ridge, Panama indentation, etc.).

7. Conclusion

The Boconó fault active during the Quaternary is recognized as a dextral sense segment. Using the offset of two thoroughly selected alluvial fans from the study area, the activity of the fault has been constrained. Calculations for the Yaritagua fan yield an age $>$ 79 ka and a lateral offset of 1350–1580 m. The maximal associated slip rate is 20 mm yr^{-1}. Based upon an age of 132–273 ka and a lateral offset of 1236–1500 m the Jaime fan shows slip rates ranging from 5.0 mm·yr^{-1} to 11.2 mm·yr^{-1}. Thus for the Boconó fault we can estimate two Pleistocene rates of $<$20.0 and 5.0–11.2 mm·yr^{-1}. These slip rates are those obtained over a longer timescale along the Boconó fault and along the fault system associated to the North Andean Block escape. By comparing our rates with geodetic rates it suggests that 40 to 100% of the deformation between the South American plate and the Maracaibo block is localized along the Boconó fault. However, it must be confirmed by carrying out complementary geodetic measurements and estimations of other slip rates along the Boconó fault and along other "slower" surrounding faults. Since the last seismic event along the studied Boconó fault segment occurred 204 years ago, and as InSAR does not show aseismic slip, we infer a slip deficit of 1 to 4 m. This implies that this Boconó fault segment could trigger a magnitude 7.0–7.6 earthquake. However, hazard assessment would require more information about the paleoseismic calendar. Finally, this study highlights the necessity to estimate slip rates on wide markers which cover the whole fault zone.

Acknowledgments

We acknowledge the two reviewers: Marie-Luce Chevalier especially for advices and comments on the discussion and figures and the anonymous reviewer for advice on the organization of the paper. We thank also J. Martinod, J.F. Ritz, and Y. Klinger for advices given in PhD comity. This work is part of the L. Pousse Beltran PhD thesis (ISTerre, USMB) funded by the French Ministry of Superior Education and Research. The authors thank the Fundacion Venezolana de Investigaciones Sismologicas (FUNVISIS) for aerial photos, topographic maps, archives of the Venezuela study area, and the logistical support given during the fieldwork. We are especially grateful to J. Oropeza, J. Aray, M. Palma, M-P. Doin and A. Singer. G. Aumaître, M. Arnold, and K. Keddadouche are thanked for their assistance during ^{10}Be measurements at the ASTER AMS national facility (CEREGE, Aix-en-Provence), which is supported by INSU/CNRS, the French Ministry of Research and Higher Education, IRD, and CEA. We acknowledge GIAME, FONACIT, and ECOS (project FONACIT-ECOS Nord PI 2009000818, FONACIT 2012002202 and 2013000361) for economical support during the field trip. This investigation was also funded by IRD, Isterre-Sud, and USBM. This work has been also supported by a grant from Labex OSUG@2020 (Investissements d'avenir-ANR10 LABX56). Pleiades images were obtained through an ISIS project funded by the CNES. We would like to thank the LPAIS (Laboratorio de Procesamiento Avanzado de Imagenes Satelitales), German Aerospace Centre (DLR), and ISIS-CNES (Incitation à l'utilisation Scientifique des Images SPOT program) for providing satellite images. We are also grateful for DEM data provided by the U.S. Geological Survey. The Global GNSS Network (GGN) is operated by UNAVCO at the direction of the Jet Propulsion Laboratory (JPL) for the National Aeronautics and Space Administration (NASA) with support from NASA under NSF Cooperative Agreement EAR-1261833. The original ALOS PALSAR data were distributed by Japan Space Systems (© METI and JAXA). We acknowledge JAXA for accepting ALOS 6th RA project PI 3223. Most of the computations presented in this paper were performed using the Froggy and Luke platform of the CIMENT infrastructure (https://ciment.ujf-grenoble.fr), which is supported by the Rhône-Alpes region (grant CPER07_13 CIRA), the OSUG@2020 Labex, and the Equip@Meso project (reference ANR-10-EQPX-29-01) of the programme Investissements d'Avenir supervised by the Agence Nationale pour la Recherche.

References

Altez, R. (2006), El desastre de 1812 en Venezuela: Sismos, vulnerabilidades y una patria no tan boba, Univ. Catolica Andres.

Alvarado, A. (2012), Néotectonique et cinématique de la déformation continentale en Equateur, PhD thesis, Univ. de Grenoble, Grenoble, Fr.

Alvarado, A., L. Audin, J. M. Nocquet, E. Jaillard, P. Mothes, P. Jarrín, M. Segovia, F. Rolandone, and D. Cisneros (2016), Partitioning of oblique convergence in the northern Andes subduction zone: Migration history and the present-day boundary of the North Andean sliver in Ecuador, *Tectonics*, *35*, 1048–1065, doi:10.1002/2016TC004117.

Anderson, R. S., J. L. Repka, and G. S. Dick (1996), Explicit treatment of inheritance in dating depositional surfaces using in situ Be-10 and Al-26, *Geology*, *24*(1), 47–51, doi:10.1130/0091-7613.

Ansberque, C., O. Bellier, V. Godard, C. Lasserre, M. Wang, R. Braucher, B. Talon, J. de Sigoyer, X. Xu, and D. L. Bourlès (2016), The Longriqu fault zone, eastern Tibetan Plateau: Segmentation and Holocene behavior, *Tectonics*, *35*, 565–585, doi:10.1002/2015TC004070.

Arnold, M., S. Merchel, D. L. Bourlès, R. Braucher, L. Benedetti, R. C. Finkel, G. Aumaître, A. Gottdang, and M. Klein (2010), The French accelerator mass spectrometry facility ASTER: Improved performance and developments, *Nucl. Instrum. Methods Phys. Res., Sect. B*, *268*(11–12), 1954–1959, doi:10.1016/j.nimb.2010.02.107.

Audemard, F. (1997), Holocene and historical earthquakes on the Boconó fault system, southern Venezuelan Andes: Trench confirmation, *J. Geodyn.*, *24*(1–4), 155–167, doi:10.1016/S0264-3707(96)00037-3.

Audemard, F. (2002), Ruptura de los grandes sismos historicos venezolanos de los siglos XIX y XX revelados por la sismicidas intrumental contemporanea, in *11° Congreso Venezolano de Géofisica*, pp. 17–20, Caracas, Venezuela.

Audemard, F. (2005), Paleoseismology in Venezuela: Objectives, methods, applications, limitations and perspectives, *Tectonophysics*, *408*(1–4), 29–61, doi:10.1016/j.tecto.2005.05.034.

Audemard, F. (2009), 5.3.8 Falla de Boconó (VE-06b y VE-06c), Atlas de deformaciones cuaternarias de los Andes, 259–271.

Audemard, F. (2014), Segmentación sismogenética de la falla de Boconó a partir de investigaciones paleosísmicas por trincheras, Venezuela occidental: ¿migración de la ruptura hacia el noreste en tiempos históricos?, *Rev. Asoc. Geol. Argent.*, *71*(2), 247–259.

Audemard, F. (2016), Paleoseismic assessment of the San Felipe segment of the Bocono fault (northwestern Venezuela): Response for the March 26th, 1812 earthquake?, *Bol. Geol.*, *38*(1), 125–149, doi:10.18273/revbol.v38n1-2016007.

Audemard, F., D. Pantosti, M. Machette, C. Costa, K. Okumura, H. Cowan, H. Diederix, and C. Ferrer (1999), Trench investigation along the Merida section of the Boconó fault (central Venezuelan Andes), Venezuela, *Tectonophysics*, *308*(1–2), 1–21, doi:10.1016/S0040-1951(99)00085-2.

Audemard, F., M. N. Machette, J. W. Cox, R. L. Dart, and K. M. Haller (2000), Map and database of quaternary faults in Venezuela and its offshore regions—Scale 1:2 000 000, Acompañado por noticia explicativa: Map and Database of Quaternary Faults in Venezuela and Offshore regions (U.S. Geol. Surv. Open File Rep., 00–18, 78 p). A project of the International Lithosphere Program Task Group II-2: Major active Faults of the World (Regional Coord.: Carlos Costa, Univ. San Luis-Argentina, ILP II-2 co-chairman Western Hemisphere: Michael Machette, U.S. Geol. Surv., Colo.), U.S. Geol. Surv. Numbered Series, 2000–18, 78 p.

Audemard, F. E., and F. Audemard (2002), Structure of Merida Andes, Venezuela: Relations with South America-Caribbean geodynamic interaction, *Tectonophysics*, *345*, 299–327.

Baquero, M., S. Grande, F. Urbani, A. Gomez, W. Reategui, D. Mendi, V. Valencia, and M. Lopéz-Martinez (2015), Petrography and geochronology of granulitic rocks from El Guayabo complex, NE Yaracuy State, Venezuela: A Meso-Neoproterozoic fragment of the Putumayo Orogen, Univ. de los Andes, Merida, Venezuela.

Beauprêtre, S., S. Garambois, I. Manighetti, and J. Malavieille (2012), Finding the buried record of past earthquakes with GPR-based palaeoseismology: A case study on the Hope fault, New Zealand, *Geophys. J. Int.*, *189*(1), 73–100, doi:10.1111/j.1365-246X.2012.05366.x.

Bellizzia, A., and D. Rodríguez (1976), Geologia del Estado de Yaracuy, in *IV Congreso Geologico Venezolano*, pp. 3317–3415.

Bellizzia, A., N. Pimentel, and R. Bajo (1976), Mapa geologico estructural de Venezuela, 1:500000, Ministerio de Minas e Hidrocarburos, Edition FONINVES.

Beltran, C. (1994), Trazas activas y síntesis neotectónica de Venezuela a escala 1: 2.000.000, in *VII Congreso Venezolano de Geofísica*, pp. 541–547, Caracas, Venezuela.

Bevington, P., and D. K. Robinson (2002), *Data Reduction and Error Analysis for the Physical Sciences*, 3rd ed., 320 pp., McGraw-Hill Higher Education, Boston.

Blard, P.-H., R. Braucher, J. Lavé, and D. Bourlès (2013), Cosmogenic ^{10}Be production rate calibrated against ^{3}He in the high tropical Andes (3800–4900 m, 20–22° S), *Earth Planet. Sci. Lett.*, *382*, 140–149, doi:10.1016/j.epsl.2013.09.010.

Braucher, R., P. Del Castillo, L. Siame, A. J. Hidy, and D. L. Bourlés (2009), Determination of both exposure time and denudation rate from an in situ-produced ^{10}Be depth profile: A mathematical proof of uniqueness. Model sensitivity and applications to natural cases, *Quat. Geochronol.*, *4*(1), 56–67, doi:10.1016/j.quageo.2008.06.001.

Braucher, R., S. Merchel, J. Borgomano, and D. L. Bourles (2011), Production of cosmogenic radionuclides at great depth: A multi element approach, *Earth Planet. Sci. Lett.*, *309*(1–2), 1–9, doi:10.1016/j.epsl.2011.06.036.

Braucher, R., V. Guillou, D. L. Bourlès, M. Arnold, G. Aumaître, K. Keddadouche, and E. Nottoli (2015), Preparation of ASTER in-house ^{10}Be/^{9}Be standard solutions, *Nucl. Instrum. Methods Phys. Res., Sect. B*, *361*, 335–340, doi:10.1016/j.nimb.2015.06.012.

Brown, E. T., J. M. Edmond, G. M. Raisbeck, F. Yiou, M. D. Kurz, and E. J. Brook (1991), Examination of surface exposure ages of Antarctic moraines using in situ produced ^{10}Be and ^{26}Al, *Geochim. Cosmochim. Acta*, *55*(8), 2269–2283, doi:10.1016/0016-7037(91)90103-C.

Bushman, J. R. (1959), Geology of the Barquisemeto area—A summary report, Asoc. Venz. Geol. Min. y Petrol., Bol. Inform.

Carcaillet, J., I. Angel, E. Carrillo, F. A. Audemard, and C. Beck (2013), Timing of the last deglaciation in the Sierra Nevada of the Mérida Andes, Venezuela, *Quat. Res.*, *80*(3), 482–494, doi:10.1016/j.yqres.2013.08.001.

Casas-Sainz, A. (1991), Estudio sismotectonico del valle de Yaracuy, informe FUNVISIS, Caracas, Venezuela.

Casas-Sainz, A. (1992), A neotectonic model for the northern sector of the Boconó fault (southern of the Caribbean plate, Venezuela), in *13 Caribbean Geological Conference*, pp. 1–19, Pinar del Rio, Cuba.

Casas-Sainz, A. (1995), Geomorphological and sedimentary features along an actives right lateral reverse fault (Yaracuy basin, Venezuela), *Z. Geomorph. N.F.*, *39*(3), 363–380.

Casas-Sainz, A., and H. Diederix (1992), El valle de Yaracuy, *Salamanca*, *4*, 269–274.

Castelltort, S., L. Goren, S. D. Willett, J.-D. Champagnac, F. Herman, and J. Braun (2012), River drainage patterns in the New Zealand Alps primarily controlled by plate tectonic strain, *Nat. Geosci.*, *5*(10), 744–748, doi:10.1038/ngeo1582.

Chevalier, M.-L., P. H. Leloup, A. Replumaz, J. Pan, D. Liu, H. Li, L. Gourbet, and M. Métois (2016), Tectonic-geomorphology of the Litang fault system, SE Tibetan Plateau, and implication for regional seismic hazard, *Tectonophysics*, doi:10.1016/j.tecto.2016.05.039.

Chmeleff, J., F. Von Blanckenburg, K. Kossert, and D. Jakob (2010), Determination of the ^{10}Be half-life by multicollector ICP-MS and liquid scintillation counting, *Nucl. Instrum. Methods Phys. Res., Sect. B*, *268*(2), 192–199, doi:10.1016/j.nimb.2009.09.012.

Chorowicz, J., P. Chotin, and R. Guillande (1996), The Garzon fault: Active southwestern boundary of the Caribbean plate in Colombia, *Geol. Rundsch.*, *85*(1), 172–179, doi:10.1007/BF00192075.

Choy, J. E., C. Palme, C. Guada, M. Morandi, and S. Klarica (2010), Macroseismic interpretation of the 1812 earthquakes in Venezuela using intensity uncertainties and a priori fault-strike information, *Bull. Seismol. Soc. Am.*, *100*(1), 241–255, doi:10.1785/0120080345.

Coello, R. (2012), Integracion geologica de la region Bobare-Farriar, entre los estados Lara y Yaracuy, Venezuela, Trabajo especial de grado, Univ. Central de Caracas, Facultad de Ingenieria. Escuela de Geologia, Minas y Geofisica, Caracas.

Colletta, B., F. Roure, B. de Toni, D. Loureiro, H. Passalacqua, and Y. Gou (1997), Tectonic inheritance, crustal architecture, and contrasting structural styles in the Venezuela Andes, *Tectonics*, *16*(5), 777–794, doi:10.1029/97TC01659.

Coplanarh (1975), *Inventario Nacional de Tierras : Estudios Geomorfologico de las Regiones Costa Noroccidental Centro Occidental y Central*, 120 pp., Ministerio de Obras Públicas, Caracas, Venezuela.

Dade, W. B., and M. E. Verdeyen (2007), Tectonic and climatic controls of alluvial-fan size and source-catchment relief, *J. Geol. Soc.*, *164*(2), 353–358, doi:10.1144/0016-76492006-039.

Davis, P. T., P. R. Bierman, K. A. Marsella, M. W. Caffee, and J. R. Southon (1999), Cosmogenic analysis of glacial terrains in the eastern Canadian Arctic: A test for inherited nuclides and the effectiveness of glacial erosion, *Ann. Glaciol.*, *28*(1), 181–188, doi:10.3189/172756499781821805.

Delmas, M., R. Braucher, Y. Gunnell, V. Guillou, M. Calvet, and D. Bourlès (2015), Constraints on Pleistocene glaciofluvial terrace age and related soil chronosequence features from vertical ^{10}Be profiles in the Ariège River catchment (Pyrenees, France), *Global Planet. Change*, *132*, 39–53, doi:10.1016/j.gloplacha.2015.06.011.

DeMets, C., R. G. Gordon, and D. F. Argus (2010), Geologically current plate motions, *Geophys. J. Int.*, *181*(1), 1–80, doi:10.1111/j.1365-246X.2009.04491.x.

de Juana, C. G., J. M. I. de Arozena, and X. P. Cadillat (1980), *Geología de Venezuela y de sus Cuencas Petrolíferas*, Foninves, Venezuela.

Dhont, D., B. Monod, Y. Hervouët, G. Backé, S. Klarica, and J. E. Choy (2012), 3D geological modeling of the Trujillo block: Insights for crustal escape models of the Venezuelan Andes, *J. S. Am. Earth Sci.*, *39*, 245–251, doi:10.1016/j.jsames.2012.04.003.

Doin, M. P., F. Lodge, S. Guillaso, R. Jolivet, C. Lasserre, G. Ducret, R. Grandin, E. Pathier, and V. Pinel (2011), Presentation of the small baseline NSBAS processing chain on a case example: The Etna deformation monitoring from 2003 to 2010 using ENVISAT data, in *Proceedings of the Fringe Symposium*, *ESA SP-697*, pp. 3434–3437, Frascati, Italy.

Dumont, J. F., E. Santana, and W. Vilema (2005), Morphologic evidence of active motion of the Zambapala fault, Gulf of Guayaquil (Ecuador), *Geomorphology*, *65*(3–4), 223–239, doi:10.1016/j.geomorph.2004.09.003.

Dunne, J., D. Elmore, and P. Muzikar (1999), Scaling factors for the rates of production of cosmogenic nuclides for geometric shielding and attenuation at depth on sloped surfaces, *Geomorphology*, *27*(1–2), 3–11, doi:10.1016/S0169-555X(98)00086-5.

Egbue, O., and J. N. Kellogg (2010), Pleistocene to present North Andean "escape", *Tectonophysics*, *489*(1), 248–257, doi:10.1016/j.tecto.2010.04.021.

Ego, F., M. Sébrier, A. Lavenu, H. Yepes, and A. Egues (1996), Quaternary state of stress in the Northern Andes and the restraining bend model for the Ecuadorian Andes, *Tectonophysics*, *259*(1–3), 101–116, doi:10.1016/0040-1951(95)00075-5.

Fattahi, M., R. T. Walker, M. M. Khatib, A. Dolati, and A. Bahroudi (2007), Slip-rate estimate and past earthquakes on the Doruneh fault, eastern Iran, *Geophys. J. Int.*, *168*(2), 691–709, doi:10.1111/j.1365-246X.2006.03248.x.

Ferrer, C. (1991), Características geomorfológicas y neotectónicas de un segmento de la falla de Boconó entre la ciudad de Mérida y la Laguna de Mucubají, Guía de la excursión. Esc. Latinoamericana de Geofísica, Estado Mérida.

Ferry, M., M. Meghraoui, N. A. Karaki, M. Al-Taj, H. Amoush, S. Al-Dhaisat, and M. Barjous (2007), A 48-kyr-long slip rate history for the Jordan Valley segment of the Dead Sea fault, *Earth Planet. Sci. Lett.*, *260*(3–4), 394–406, doi:10.1016/j.epsl.2007.05.049.

Fialko, Y. (2006), Interseismic strain accumulation and the earthquake potential on the southern San Andreas fault system, *Nature*, *441*(7096), 968–971, doi:10.1038/nature04797.

Frankel, K. L., L. A. Owen, J. F. Dolan, J. R. Knott, Z. M. Lifton, R. C. Finkel, and T. Wasklewicz (2015), Timing and rates of Holocene normal faulting along the Black Mountains fault zone, Death Valley, USA, *Lithosphere*, L464.1, doi:10.1130/L464.1.

Giegengack, R., R. Grauch, and R. Shagam (1976), Geometry of late Cenozoic displacement along the Bocono fault, Venezuelan Andes, *Bol. Geol. Publ. Espec.*, *7*(2), 1201–1223.

Giraldo, C. (1985), *Neotectonique et Sismotectonique de la Region d'El Tocuyo San Felipe (Venezuela Centro Occidental)*, Univ. des Sciences et Techniques du Languedoc, France.

Gold, R. D., N. G. Reitman, R. W. Briggs, W. D. Barnhart, G. P. Hayes, and E. Wilson (2015), On- and off-fault deformation associated with the September 2013 M_w 7.7 Balochistan earthquake: Implications for geologic slip rate measurements, *Tectonophysics*, doi:10.1016/j.tecto.2015.08.019.

González, O., Z. Millán, and M. Bezada (2008), Pedogénesis de una cronosecuencia de suelos en la región de Yaritagua y Guama, estado Yaracuy-Venezuela, *Rev. Geogr. Venez.*, *49*(2), 223–245.

González, O., M. Bezada, and Z. Millán (2012), Geomorfología de los sistemas de abanicos aluviales localizados en el trayecto Yaritagua-Guama, estado Yaracuy-Venezuela, *Rev. Geogr. Venez.*, *53*(2), 255–276.

Gosse, J. C., and F. M. Phillips (2001), Terrestrial in situ cosmogenic nuclides: Theory and application, *Quat. Sci. Rev.*, *20*(14), 1475–1560, doi:10.1016/S0277-3791(00)00171-2.

Grases, J. (1980), *Investigación sobre los Sismos Destructores que Han Afectado el Occidente y el Centro de Venezuela*, vol. 3, INTEVEP, Caracas, Venezuela.

Graveleau, F., V. Strak, S. Dominguez, J. Malavieille, M. Chatton, I. Manighetti, and C. Petit (2015), Experimental modelling of tectonics–erosion–sedimentation interactions in compressional, extensional, and strike–slip settings, *Geomorphology*, doi:10.1016/j.geomorph.2015.02.011.

Gupta, H. K., N. P. Rao, B. K. Rastogi, and D. Sarkar (2001), The deadliest intraplate earthquake, *Science*, *291*(5511), 2101–2102, doi:10.1126/science.1060197.

Heisinger, B., D. Lal, A. J. T. Jull, P. Kubik, S. Ivy-Ochs, K. Knie, and E. Nolte (2002a), Production of selected cosmogenic radionuclides by muons: 2. Capture of negative muons, *Earth Planet. Sci. Lett.*, *200*(3–4), 357–369, doi:10.1016/S0012-821X(02)00641-6.

Heisinger, B., D. Lal, A. J. T. Jull, P. Kubik, S. Ivy-Ochs, S. Neumaier, K. Knie, V. Lazarev, and E. Nolte (2002b), Production of selected cosmogenic radionuclides by muons: 1. Fast muons, *Earth Planet. Sci. Lett.*, *200*(3–4), 345–355, doi:10.1016/S0012-821X(02)00640-4.

Hernandez S, A. C. (2013), Integracion geologica de la region Bobare-San Felipe, Estado Lara y Yaracuy, Venezuela, Trabajo especial de grado, Univ. Central de Caracas, Facultad de Ingenieria. Escuela de Geologia, Minas y Geofisica, Caracas.

Hidy, A. J., J. C. Gosse, J. L. Pederson, J. P. Mattern, and R. C. Finkel (2010), A geologically constrained Monte Carlo approach to modeling exposure ages from profiles of cosmogenic nuclides: An example from Lees Ferry, Arizona, *Geochem. Geophys. Geosyst.*, *11*, Q0AA10, doi:10.1029/2010GC003084.

International Seismological Centre (2013), *On-line Bulletin*, Int. Seismol. Cent., Thatcham, U. K.

Kellogg, J. N., V. Vega, T. C. Stailings, and C. L. V. Aiken (1995), Tectonic development of Panama, Costa Rica, and the Colombian Andes: Constraints from Global Positioning System geodetic studies and gravity, *Geol. Soc. Am. Spec. Pap.*, *295*, 75–90, doi:10.1130/SPE295-p75.

Kelly, M. A., T. V. Lowell, P. J. Applegate, F. M. Phillips, J. M. Schaefer, C. A. Smith, H. Kim, K. C. Leonard, and A. M. Hudson (2013), A locally calibrated, late glacial ^{10}Be production rate from a low-latitude, high-altitude site in the Peruvian Andes, *Quat. Geochronol.*, doi:10.1016/j.quageo.2013.10.007.

Klinger, Y., X. Xu, P. Tapponnier, J. V. der Woerd, C. Lasserre, and G. King (2005), High-resolution satellite imagery mapping of the surface rupture and slip distribution of the M_w ~7.8, 14 November 2001 Kokoxili earthquake, Kunlun fault, northern Tibet, China, *Bull. Seismol. Soc. Am.*, *95*(5), 1970–1987, doi:10.1785/0120040233.

Korschinek, G., et al. (2010), A new value for the half-life of Be-10 by heavy-ion elastic recoil detection and liquid scintillation counting, *Nucl. Instrum. Methods Phys. Res., Sect. B*, *268*(2), 187–191, doi:10.1016/j.nimb.2009.09.020.

Lal, D. (1991), Cosmic ray labeling of erosion surfaces: In situ nuclide production rates and erosion models, *Earth Planet. Sci. Lett.*, *104*(2–4), 424–439, doi:10.1016/0012-821X(91)90220-C.

Manighetti, I., C. Caulet, L. De Barros, C. Perrin, F. Cappa, and Y. Gaudemer (2015), Generic along-strike segmentation of afar normal faults, East Africa: Implications on fault growth and stress heterogeneity on seismogenic fault planes, *Geochem. Geophys. Geosyst.*, *16*, 443–467, doi:10.1002/2014GC005691.

Martin, L. C. P., P.-H. Blard, J. Lavé, R. Braucher, M. Lupker, T. Condom, J. Charreau, V. Mariotti, ASTER Team, and E. Davy (2015), In situ cosmogenic 10Be production rate in the high tropical Andes, *Quat. Geochronol.*, doi:10.1016/j.quageo.2015.06.012.

McGill, S. F., and K. Sieh (1991), Surficial offsets on the central and eastern Garlock fault associated with prehistoric earthquakes, *J. Geophys. Res.*, *96*(B13), 21,597–21,621, doi:10.1029/91JB02030.

Merchel, S., and U. Herpers (1999), An update on radiochemical separation techniques for the determination of long-lived radionuclides via accelerator mass spectrometry, *Ract*, *84*(4), 215–220, doi:10.1524/ract.1999.84.4.215.

Monod, B., D. Dhont, and Y. Hervouët (2010), Orogenic float of the Venezuelan Andes, *Tectonophysics*, *490*(1–2), 123–135, doi:10.1016/j.tecto.2010.04.036.

Mora-Páez, H., D. J. Mencin, P. Molnar, H. Diederix, L. Cardona-Piedrahita, J.-R. Peláez-Gaviria, and Y. Corchuelo-Cuervo (2016), GPS velocities and the construction of the eastern cordillera of the Colombian Andes, *Geophys. Res. Lett.*, *43*, 8407–8416, doi:10.1002/2016GL069795.

Moratto, Z. M., M. J. Broxton, R. A. Beyer, M. Lundy, and K. Husmann (2010), Ames stereo pipeline, NASA's open source automated Stereogrammetry software, in *Lunar and Planetary Science Conference*, vol. 41, p. 2364.

Nevado, F. (2012), Integracion geologica de la region Moroturo -Palmasola, Estado Yaracuy y Lara, Venezuela, Trabajo especial de grado, Univ. Central de Caracas, Facultad de Ingenieria. Escuela de Geologia, Minas y Geofisica, Caracas.

Newman, A., S. Stein, J. Weber, J. Engeln, A. Mao, and T. Dixon (1999), Slow deformation and lower seismic hazard at the New Madrid seismic zone, *Science*, *284*(5414), 619–621, doi:10.1126/science.284.5414.619.

Nishiizumi, K., M. Imamura, M. W. Caffee, J. R. Southon, R. C. Finkel, and J. McAninch (2007), Absolute calibration of Be-10 AMS standards, *Nucl. Instrum. Methods Phys. Res., Sect. B*, *258*(2), 403–413, doi:10.1016/j.nimb.2007.01.297.

Peltzer, G., P. Tapponnier, Y. Gaudemer, B. Meyer, S. Guo, K. Yin, Z. Chen, and H. Dai (1988), Offsets of Late Quaternary morphology, rate of slip, and recurrence of large earthquakes on the Changma fault (Gansu, China), *J. Geophys. Res.*, *93*(B7), 7793–7812, doi:10.1029/JB093iB07p07793.

Pennington, W. D. (1981), Subduction of the eastern Panama Basin and seismotectonics of northwestern South America, *J. Geophys. Res.*, *86*(B11), 10,753–10,770, doi:10.1029/JB086iB11p10753.

Pérez, O. J., R. Bilham, R. Bendick, J. R. Velandia, N. Hernández, C. Moncayo, M. Hoyer, and M. Kozuch (2001), Velocity field across the southern Caribbean plate boundary and estimates of Caribbean/south-American plate motion using GPS geodesy 1994–2000, *Geophys. Res. Lett.*, *28*(15), 2987–2990, doi:10.1029/2001GL013183.

Pérez, O. J., R. Bilham, and M. Sequera (2011), GPS derived velocity field in western Venezuela: Dextral shear component associated to the Boconó fault and convergent component normal to the Andes, *Interciencia*, *26*(2), 69–74.

Pousse Beltran, L., E. Pathier, F. Jouanne, R. Vassallo, C. Reinoza, F. Audemard, M. P. Doin, and M. Volat (2016), Spatial and temporal variations in creep rate along the El Pilar fault at the Caribbean-south American plate boundary (Venezuela), from InSAR, *J. Geophys. Res. Solid Earth*, *121*, 8276–8296, doi:10.1002/2016JB013121.

Putkonen, J., and T. Swanson (2003), Accuracy of cosmogenic ages for moraines, *Quat. Res.*, *59*(2), 255–261, doi:10.1016/S0033-5894(03)00006-1.

Reinoza, C. E. (2014), Application de la géodésie satellitaire GNSS à haute résolution à la déformation de la marge Sud-Caraïbe. Implication pour l'aléa sismique dans l'Ouest et le Nord-Est du Venezuela, PhD thesis, Univ. Joseph Fourier / Univ. de Savoie Mont - Blanc, Chambéry, 15 Dec.

Reinoza, C. E., F. Jouanne, F. Audemard, M. Schmitz, and C. Beck (2015), Geodetic exploration of strain along the El Pilar fault in northeastern Venezuela, *J. Geophys. Res. Solid Earth*, *120*, 1993–2013, doi:10.1002/2014JB011483.

Ritz, J.-F., E. T. Brown, D. L. Bourlès, H. Philip, A. Schlupp, G. M. Raisbeck, F. Yiou, and B. Enkhtuvshin (1995), Slip rates along active faults estimated with cosmic-ray–exposure dates: Application to the Bogd fault, Gobi-Altaï, Mongolia, *Geology*, *23*(11), 1019–1022, doi:10.1130/0091-7613(1995)023<1019:SRAAFE>2.3.CO;2.

Ritz, J.-F., D. Bourles, E. T. Brown, S. Carretier, J. Chery, and B. Enhtuvshin (2003), Late Pleistocene to Holocene slip rates for the Gurvan Bulag thrust fault (Gobi-Altay, Mongolia) estimated with 10 Be dates, *J. Geophys. Res.*, *108*(B3), 2162, doi:10.1029/2001JB000553.

Rizza, M., J. F. Ritz, C. Prentice, R. Vassallo, R. Braucher, and C. Larroque (2015), Earthquake geology of the Bulnay fault (Mongolia), *Bull. Seismol. Soc. Am.*, *105*(1), 72–93, doi:10.1785/0120140119.

Rockwell, T. K., and Y. Klinger (2013), Surface rupture and slip distribution of the 1940 Imperial Valley earthquake, imperial fault, Southern California: Implications for rupture segmentation and dynamics, *Bull. Seismol. Soc. Am.*, *103*(2A), 629–640, doi:10.1785/0120120192.

Rockwell, T. K., S. Lindvall, T. Dawson, R. Langridge, W. Lettis, and Y. Klinger (2002), Lateral offsets on surveyed cultural features resulting from the 1999 İzmit and Düzce earthquakes, Turkey, *Bull. Seismol. Soc. Am.*, *92*(1), 79–94, doi:10.1785/0120000809.

Rod, E. (1956), Strike-slip faults of northern Venezuela, *Bull. Am. Assoc. Pet. Geol.*, *40*, 457–476.

Ruszkiczay-Rüdiger, Z., R. Braucher, Á. Novothny, G. Csillag, L. Fodor, G. Molnár, and B. Madarász (2016), Tectonic and climatic control on terrace formation: Coupling in situ produced ^{10}Be depth profiles and luminescence approach, Danube River, Hungary, Central Europe, *Quat. Sci. Rev., Part A*, *131*, 127–147, doi:10.1016/j.quascirev.2015.10.041.

Ryder, I., and R. Bürgmann (2008), Spatial variations in slip deficit on the central San Andreas fault from InSAR, *Geophys. J. Int.*, *175*(3), 837–852, doi:10.1111/j.1365-246X.2008.03938.x.

Salgado-Labouriau, M. L., C. Schubert, and J. Sam Valastro (1977), Paleoecologic analysis of a late-quaternary terrace from Mucubaji, Venezuelan Andes, *J. Biogeogr.*, *4*(4), 313–325, doi:10.2307/3038190.

Scharer, K. M., J. B. Salisbury, J. R. Arrowsmith, and T. K. Rockwell (2014), Southern San Andreas fault evaluation field activity: Approaches to measuring small geomorphic offsets—Challenges and recommendations for active fault studies, *Seismol. Res. Lett.*, *85*(1), 68–76, doi:10.1785/0220130108.

Schubert, C. (1982), Neotectonics of Boconó fault, western Venezuela, *Tectonophysics*, *85*(3–4), 205–220, doi:10.1016/0040-1951(82)90103-2.

Schubert, C. (1983), La cuenca de Yaracuy: Una estructura neotectonica en la region centro occidental de Venezuela, *Geol. Norandina*, *8*, 194–202.

Shelef, E., and M. Oskin (2010), Deformation processes adjacent to active faults: Examples from eastern California, *J. Geophys. Res.*, *115*, B05308, doi:10.1029/2009JB006289.

Shirzaei, M., R. Bürgmann, and T. Taira (2013), Implications of recent asperity failures and aseismic creep for time-dependent earthquake hazard on the Hayward fault, *Earth Planet. Sci. Lett.*, *371–372*, 59–66, doi:10.1016/j.epsl.2013.04.024.

Siame, L., O. Bellier, R. Braucher, M. Sébrier, M. Cushing, and D. Bourlès (2004), Local erosion rates versus active tectonics: Cosmic ray exposure modelling in Provence (south-east France), *Earth Planet. Sci. Lett.*, *220*(3–4), 345–364, doi:10.1016/S0012-821X(04)00061-5.

Singer, A., and C. Beltran (1996), Active faulting in the southern Venezuelan Andes and Colombian borderland, in *3rd International Symposium on Andean Geodynamics*, pp. 243–246, Saint - Malo.

Soulas, J. P. (1986), Neotectónica y tectónica den Venezuela, in *6° Congreso Geológico Venezolano*, *Mem.*, vol. 10, pp. 6639–6656, Caracas, Venezuela.

Stone, J. O. (2000), Air pressure and cosmogenic isotope production, *J. Geophys. Res.*, *105*(B10), 23,753–23,759, doi:10.1029/2000JB900181.

Symithe, S., E. Calais, J. B. de Chabalier, R. Robertson, and M. Higgins (2015), Current block motions and strain accumulation on active faults in the Caribbean, *J. Geophys. Res. Solid Earth*, *120*, 3748–3774, doi:10.1002/2014JB011779.

Tibaldi, A., A. Rovida, and C. Corazzato (2007), Late quaternary kinematics, slip-rate and segmentation of a major cordillera-parallel transcurrent fault: The Cayambe-Afiladores-Sibundoy system, NW South America, *J. Struct. Geol.*, *29*(4), 664–680, doi:10.1016/j.jsg.2006.11.008.

Trenkamp, R., J. N. Kellogg, J. T. Freymueller, and H. P. Mora (2002), Wide plate margin deformation, southern central America and northwestern South America, CASA GPS observations, *J. S. Am. Earth Sci.*, *15*(2), 157–171, doi:10.1016/S0895-9811(02)00018-4.

University NAVSTAR Consortium (UNAVCO) (2017), GPS Velocity Viewer | software | UNAVCO. [Available at https://www.unavco.org/software/visualization/GPS-Velocity-Viewer/GPS-Velocity-Viewer.html, (Accessed 9 January 2017).]

Urbani, F. (2008), Revision de la nomenclatura de las unidades de rocas igneas y metamorfica del Norte de Venezuela, *Bol. Acad. C. Fis., Mat. Nat.*, *68*(3), 27–43.

Urbani, F. (2014), *Geologia de la Region Septentrional de los Estados Lara et Yaracuy*, Funvisis, Caracas, Venezuela.

U.S. Geological Survey (2017), ANSS comprehensive catalog (ComCat). [Available at http://earthquake.usgs.gov/earthquakes/search, (Accessed 9 January 2017).]

Van der Woerd, J., P. Tapponnier, and F. J. Ryerson (2002), Uniform postglacial slip rate along the central 600 km of the Kunlun fault (Tibet), from ^{26}Al ^{10}Be and ^{14}C dating of risers offsets, and climatic origin of the regional morphology, *Geophys. J. Int.*, *148*, 336–388.

Veihmeyer, F., and A. Hendrickson (1948), Soil density and root penetration, *Soil Sci.*, *65*(6), 487–494.

Weber, J. C., T. H. Dixon, C. DeMets, W. B. Ambeh, P. Jansma, G. Mattioli, J. Saleh, G. Sella, R. Bilham, and O. Pérez (2001), GPS estimate of relative motion between the Caribbean and South American plates, and geologic implications for Trinidad and Venezuela, *Geology*, *29*(1), 75–78, doi:10.1130/0091-7613(2001)029<0075:GEORMB>2.0.CO;2.

Wells, D. L., and K. J. Coppersmith (1994), New empirical relationships among magnitude, rupture length, rupture width, rupture area, and surface displacement, *Bull. Seismol. Soc. Am.*, *84*(4), 974–1002.

Wesnousky, S. G., R. Aranguren, M. Rengifo, L. A. Owen, M. W. Caffee, M. K. Murari, and O. J. Pérez (2012), Toward quantifying geomorphic rates of crustal displacement, landscape development, and the age of glaciation in the Venezuelan Andes, *Geomorphology*, *141–142*, 99–113, doi:10.1016/j.geomorph.2011.12.028.

Winter, T., J.-P. Avouac, and A. Lavenu (1993), Late quaternary kinematics of the Pallatanga strike-slip fault (Central Ecuador) from topographic measurements of displaced morphological features, *Geophys. J. Int.*, *115*(3), 905–920, doi:10.1111/j.1365-246X.1993.tb01500.x.

Witt, C., and J. Bourgois (2010), Forearc basin formation in the tectonic wake of a collision-driven, coastwise migrating crustal block: The example of the North Andean block and the extensional Gulf of Guayaquil-Tumbes Basin (Ecuador-Peru border area), *Geol. Soc. Am. Bull.*, *122*(1–2), 89–108, doi:10.1130/B26386.1.

Yano, T. E., G. Shao, Q. Liu, C. Ji, and R. J. Archuleta (2014), Coseismic and potential early afterslip distribution of the 2009 M_w 6.3 L'Aquila, Italy earthquake, *Geophys. J. Int.*, *199*(1), 23–40, doi:10.1093/gji/ggu241.

Yeats, R. S., and C. S. Prentice (1996), Introduction to special section: Paleoseismology, *J. Geophys. Res.*, *101*(B3), 5847–5853, doi:10.1029/95JB03134.

Zielke, O., Y. Klinger, and J. R. Arrowsmith (2015), Fault slip and earthquake recurrence along strike-slip faults—Contributions of high-resolution geomorphic data, *Tectonophysics*, *638*, 43–62, doi:10.1016/j.tecto.2014.11.004.

Zinke, R., J. Hollingsworth, and J. F. Dolan (2014), Surface slip and off-fault deformation patterns in the 2013 M_w 7.7 Balochistan, Pakistan earthquake: Implications for controls on the distribution of near-surface coseismic slip, *Geochem. Geophys. Geosyst.*, *15*, 5034–5050, doi:10.1002/2014GC005538.